An active atmospheric methane sink in high Arctic mineral cryosols

Authors: M.C.Y. Lau[1]*, B.T. Stackhouse[1], A.C. Layton[2], A. Chauhan[2], T.A. Vishnivetskaya[2], K. Chourey[3], N.C.S. Mykytczuk[4], P.C. Bennett[5], G. Lamarche-Gagnon[4], N. Burton[1], J. Ronholm[4], W.H. Pollard[4], C.R. Omelon[5], D.M. Medvigy[1], R.L. Hettich[3], S.M. Pfiffner[2], L.G. Whyte[3]. and T.C. Onstott[1]

Affiliations:

[1]Department of Geosciences, Princeton University, Princeton, NJ 08544, USA.

[2]University of Tennessee, Knoxville, TN, USA.

[3]ORNL, Oak Ridge, TN, USA.

[4]McGill University, Quebec, Canada.

[5]University of Texas, Austin, TX, USA.

*Correspondence to: maglau@princeton.edu

Abstract:

The transition of Arctic carbon-rich cryosols into methane (CH_4)-emitting wetlands due to global warming is a rising concern. However, the spatially predominant mineral cryosols and their CH_4 emission potential are poorly understood. Fluxes measured *in situ* and estimated under laboratory conditions coupled with -omics analysis indicate (1) mineral cryosols in the Canadian high Arctic contain atmospheric CH_4-oxidizing bacteria; (2) the atmospheric CH_4 uptake flux increases with ground temperature; and, as a result, (3) the atmospheric CH_4 sink strength will increase by a factor of 5-30 as the Arctic warms by 5-15°C over a century. We demonstrated that acidic mineral cryosols have previously unrecognized potential of negative CH_4 feedback.

Main Text:

After 7 years of steady-state concentration between 1999 and 2006, atmospheric (atm) CH_4 has been increasing steadily at 5 ppb yr^{-1} (*1*, *2*). At 1.81 ppmv in 2011, the atm CH_4 concentration is 216 times lower than that of carbon dioxide (CO_2), however, it accounts for 18% of the total radiative forcing by long-lived greenhouse gases (GHG) (*2*) and has a global warming potential 75 times greater than CO_2 over a 20-year timescale (*3*). Alleviation of atm CH_4 level is, therefore, one of the important avenues to address global warming. Although cost-effective strategies could be applied to mitigate CH_4 production by anthropogenic activities (~64% of post-industrial total CH_4 emissions), the future global CH_4 budget will depend greatly on the uncertain responses of natural

ecosystems to climate change, especially in wetlands and permafrost-affected areas in the Arctic and sub-Arctic regions (*4*, *5*).

Permafrost, defined as "ground that remains at or below 0°C for at least two consecutive years" (*6*), is overlain by an active layer that thaws seasonally. By 2100, it is projected that the mean annual air temperature in the Arctic will have increased by up to 6°C (*7*) which would result in the thawing of more than 75% of the 13 – 15 x10^6 km^2 of permafrost (north of 45°N) (*8*, *9*) down to 3.5 m (*10*). This volume, accounting for 44% of global soil carbon (*10*), will become available for microbial mineralization into GHG will amplify warming. As a result of the concern about this positive feedback response, the transition of carbon-rich permafrost into CH_4-emitting wetlands has been the focus of considerable research (Fig. 1, 1-7) even though the majority (81%) of Arctic permafrost is comprised of mineral (carbon-poor) cryosols. In the present study, we investigated the CH_4 feedback response to water saturation and temperature of representative mineral cryosols on Axel Heiberg Island (AHI) in the Canadian high Arctic by both *in situ* flux measurements and laboratory experiments and also evaluated how these cryosols would respond to changing climate.

The study site (79°24"57'N, 90°45"46'W) near Expedition Fjord is characterized by high-centered ice-wedge polygons of sub-neutral pH tundra. Measurement of *in situ* surface CH_4 flux during initial thaw and mid-summer from 2011 to 2013 consistently showed atm CH_4 uptake at various localities (Fig. 1a). Observation of atm CH_4 uptake was reported in Alaskan permafrost sites in early 1990s (*11*). Since then negative CH_4 flux was only occasionally recorded in other permafrost-affected sites including cryosols

of high carbon and water saturation where CH_4 emission was expected (Fig. 1, b-h; Table S1). The CH_4 uptake rates at AHI (-0.1 to -0.8 mg CH_4-C m^{-2} day^{-1}) are at the lower end of the range (-0.02 to -17.8 mg CH_4-C m^{-2} day^{-1}) observed among other sites in the Arctic and sub-Arctic region (Fig. 1, a-h) but comparable to that of other terrestrial systems at lower latitudes (-0.1 to -1.0 mg CH_4-C m^{-2} day^{-1}) (*12*). The comparison to the scarce data of CH_4 uptake at the northern latitudes suggests that acidic mineral cryosols act as a constant active CH_4 sink as a result of low pH, low vegetation cover, low water saturation and low carbon availability (Table S1).

Atm CH_4 oxidation primarily occurs by reacting with hydroxyl radicals (OH•) in the troposphere and stratosphere but is also mediated by atmospheric MOB, aerobic CH_4-oxidizing bacteria that have high affinity for atm CH_4 (atmMOB) (*4*) Metagenomic data of near-surface cryosols revealed known methanotrophic taxa comprising about 0.7% of total sequences with a-Proteobacterial (Type II) methanotrophs dominating over g-Proteobacterial (Type I) or Verrucomicrobial methanotrophs (Table S2). The abundance of methanotrophic community decreased with depth (*13*). Since genetic information of atmMOB has been limited to a collection of *pmo*A genes encoding for the α subunit of particulate methane monooxygenase (pMMO) (*14–16*) and a 42 kb-long sequence of genotype USCα (*17*), the search for *pmo* genes has been the only way to detect the yet-to-be cultured atmMOB whose phylogenetic identity of 16S rRNA gene has not yet been revealed.

De novo co-assembly of raw sequences obtained 13 contigs that contained genes affiliated to MMO and homologous enzymes (Table S3). Six of which (528-1301 nt)

yielded 7 *pmo* gene fragments, as one comprised a section of *pmo*C and *pmo*A genes. Although this approach has masked the within and inter-library genetic variations, the resultant contigs represent the dominant taxa. The phylogeny of *pmo*A and *pmo*C genes (Fig. S1-3) suggests that the prevalent pMMO-possessing MOB are closely related to atmMOB genotype Upland Soil Cluster a (USCa), which appears to be dominant in low pH soils such as these samples (pH 5.5 – 6) (*15*, *17*). While USCa is likely responsible for most of the observed CH_4 uptake, the contribution from other MOB is not excluded as it has been shown that some are able to oxidize CH_4 at atmospheric concentration by expressing high-affinity pMMO (*18*) or when supplemented with methanol (*19*).

Queries for *pmo* genes in our 10 metagenome libraries showed extremely low abundance of *pmo* genes (Table S3), which implied the percentage of pMMO proteins in these samples to be similarly low. Nonetheless, proteome profiling of near-surface cryosols led to identification of PmoB proteins (Table S4) where the copper active site is located (*20*). PmoB subunits have been detected more frequently than other two subunits in CH_4-oxidizing samples (*21*) which suggested that β subunits of pMMO may serve a regulator role same as those of the soluble form of MMO (*22*).

Without this unprecedentedly extensive sequencing effort, it would have been unlikely to detect these minority gene populations and identify the encoded proteins. Technical problems such as insufficient sequencing depth in metagenomic analyses and primer bias in PCR-based assays (*23*) partly explain why atmMOB has not been reported in previous molecular studies carried out in the Arctic region (Table S5). Further, previous studies were not designed to search for atmMOB. To the knowledge of authors,

this first report of USCα in metagenome libraries indicated our data representing the largest inventory of USCα genomes which will facilitate the search for additional USCα genes and hence improve the identification of its phylogenetic lineage. The detection of atmMOB at AHI (this study and (*15*)) indicates that upland mineral cryosols are a previously unidentified habitat of atmMOB (*17*) and the biogeographic range of this methanotrophic group is wide and extends poleward.

CH_4 uptake by AHI active layer cryosols was reproducible under laboratory conditions. A factorial microcosm experiment simulating natural thaw conditions was designed to study effects of water saturation and temperature on atm CH_4 oxidation. CH_4 (initial concentration at 2.0 ppmv) was consumed under all conditions by the end of a 31-day incubation (Table S6). Assuming a first-order rate law (*11*), estimated CH_4 oxidation rates were threefold faster at 33% saturation than at 100% saturation and twofold faster at 10°C than at 4°C (Table 1). Thermal sensitivity of atm CH_4 oxidation was quantitatively assessed using the temperature coefficient (Q_{10}), which describes the rate of change of a reaction resulting from an increment of 10°C. At 66% and 100% saturation, the Q_{10} values were within the range of 1.3 to 2.9 reported from previous incubation experiments carried out at atmospheric or elevated concentrations of CH_4 (Fig. 2). In contrast, the Q_{10} value was 8 at 33% saturation (Fig. 2). This lower water saturation not only increased the CH_4 oxidation rate, presumably by promoting the availability of oxygen to atmMOB, but also allowed atmMOB to be more responsive to temperature change. A similar interactive effect of water saturation and temperature on atm CH_4 oxidation was observed in boreal forest soils (*24*). High Q_{10} values were also estimated for CH_4 oxidation in Siberian

124 cryosols at elevated CH_4 concentrations (Fig. 2), suggesting that under some conditions
125 thermal sensitivity of CH_4 oxidation is as high as that reported for methanogenesis, which
126 exhibits Q_{10} values of 0.6 to 12, in some boreal and temperate wetlands (*25*).

127 Methanogens were present at the lowest abundance (1.6% of total sequences) in
128 near-surface cryosols (Table S6 and (*13*)) where oxic conditions are inhibitory to
129 methanogenesis. Depth profiling of dissolved CH_4 in AHI thawed cores showed that
130 methanogenesis took place at depths near the permafrost table at 4°C; however, pore
131 water CH_4 concentrations diminished towards the surface and became undetectable at 5
132 cm (*13*). *In situ* depth profiling of pore gas showed progressively decreasing CH_4
133 concentration with depth, with a minimum concentration less than 20 ppbv. These results
134 demonstrated that CH_4 produced at depth was completely oxidized before reaching the
135 atmosphere. Since AHI active layer cryosols were a consistent CH_4 sink upon thawing,
136 we established an Arrhenius relationship between *in situ* atm CH_4 uptake and
137 corresponding surface soil temperature to investigate temperature dependence of atm CH_4
138 oxidation under native conditions.

139 Castro *et al*. reported CH_4 uptake increased with increasing ground temperature
140 up to 10°C and plateaued between 10 and 20°C (*26*). Atm CH_4 uptake at AHI displayed
141 different kinetic properties as a function of temperature (Fig. 3), similar to . However, the
142 breakpoint of temperature response occurred at a lower temperature (5.6°C) and the rate
143 of increase was reduced at temperatures higher than 5.6°C. A stronger thermal sensitivity
144 of atm CH_4 uptake over cooler temperatures suggests that atmMOB at high northern
145 latitudes may contain pMMO adapted to cold environments.

Based on this temperature-dependent flux behavior (Fig. 3), we estimated the monthly and annual CH_4 uptake fluxes at AHI at air temperatures simulated for this location using multiple climate models as well as those projected from observations at nearby Eureka, Ellesmere Island in 2011. Climate models predicted a seasonal difference in warming over the century, with 10-14°C warming in fall/winter and 3-5°C warming in spring/summer (Fig. S4). As a consequence, CH_4 uptake fluxes would take place over longer time periods each year, which then would result in a 5-fold increase in the annual CH_4 uptake (-1.8 mg CH_4-C m^{-2} $year^{-1}$) (Table 1). However, the mean summer temperatures simulated for the 2090s were 5-10°C cooler than those observed in 2011 (Fig. S4). This summer warming further increased the annual uptake fluxes by a factor of 4 to 6 (-8.0 to -11.5 mg CH_4-C m^{-2} $year^{-1}$) (Table 1). Although 2011 could have been an abnormally warm year (field observations and (*27*)), this indicates that warming of 10°C at the Arctic across all months is possible (Fig. S4). Under expected patterns of climate change, AHI will continue to be a microbial atm CH_4 sink and the sink strength will vary distinctly in accordance with seasonal and inter-annual temperature variability. We recommend this 2-kinetics temperature-dependence of atm CH_4 uptake be implemented in CH_4 flux modeling to improve predictive power.

Net CH_4 flux in soils is a balance between methanogenesis and CH_4 oxidation where both reactions are sensitive to temperature change. It may then be a concern that future warming may convert our study site from a sink of CH_4 to a source if methanogenesis is enhanced relative to methanotrophy as soil temperature increases. Since a decreasing temperature gradient as a function of depth will exist down to the

permafrost table, (atm) CH_4 oxidation in the upper layers is anticipated to be greater than methanogenesis at lower depths. AHI should continue to be a CH_4 sink under this assumption. Nonetheless, further investigations are required to determine: (i) the range of CH_4 concentrations that the methanotrophic community can accommodate before saturation by subsurface methanogenesis; (ii) the critical conditions (e.g. temperature and water saturation level) under which this offset takes place; and (iii) changes in permafrost dynamics as well as the potential topographical and hydrological modifications as a result of warming.

If atmMOB are ubiquitous in mineral cyrosols (and potentially present in peatlands), permafrost-affected cryosols (and particularly mineral cryosols) have likely been modulating the rate of atm CH_4 increase. Further studies are required to determine the impact on the regional CH_4 fluxes, for example, (i) if the uptake of atm CH_4 during summer months accounts for the dip of ~50 ppbv in atm CH_4 concentration and the $\delta^{13}C$ enrichment observed seasonally in summer at high latitudes (*1*, *28*, *29*) and (ii) whether a CH_4 sink at high latitudes attributes to the unexplained bowl-shape variation in the CH_4 isotopic record across the Holocene period (*30*).

To conclude, this work presents the first evidence of atm CH_4 uptake in mineral cryosols in the Canadian high Arctic by active atmMOB and that their thermal sensitivity indicates atm CH_4 uptake is enhanced under global warming. This study calls attention to the wide geographic distribution of atmMOB, as well as the significance of atm CH_4 microbial oxidation in the context of regional CH_4 flux models and global warming.

References and Notes:

1. E. J. Dlugokencky *et al.*, Observational constraints on recent increases in the atmospheric CH4 burden, *Geophys. Res. Lett.* **36**, L18803 (2009).

2. *WMO Greenhouse Gas Bulletin: The State of Greenhouse Gases in the Atmosphere Based on Global Observations through 2011* (2012), p. No. 8.

3. D. T. Shindell *et al.*, Improved attribution of climate forcing to emissions., *Science (80-.).* **326**, 716–718 (2009).

4. E. J. Dlugokencky, E. G. Nisbet, R. Fisher, D. Lowry, Global atmospheric methane: budget, changes and dangers, *Philos. Trans. A. Math. Phys. Eng. Sci.* **369**, 2058–2072 (2011).

5. D. E. Graham *et al.*, Microbes in thawing permafrost: the unknown variable in the climate change equation, *ISME Journal. J.* **6**, 709–712 (2012).

6. R. O. Van Everdingen, Ed., *Multi-language Glossary of Permafrost and Related Ground-ice Terms* (National Snow and Ice Data Center/World Data Center for Glaciology, Boulder, CO).

7. IPCC, *Climate Change 2007: The Physical Science Basis. Contribution of Working Group I to the Fourth Assessment Report of the Intergovernmental Panel on Climate Change* S. Solomon *et al.*, Eds. (Cambridge University Press, Cambridge, United Kingdom and New York, NY, USA, 2007).

8. C. Tarnocai *et al.*, Soil organic carbon pools in the northern circumpolar permafrost region, *Glob. Biogeochemcial Cycles* **23**, doi:10.1029/2008GB003327 (2009).

9. T. Zhang, R. G. Barry, K. Knowles, J. a. Heginbottom, J. Brown, Statistics and characteristics of permafrost and ground-ice distribution in the Northern Hemisphere, *Polar Geogr.* **31**, 47–68 (2008).

209 10. D. M. Lawrence, A. G. Slater, V. E. Romanovsky, D. J. Nicolsky, Sensitivity of a model projection of
210 near-surface permafrost degradation to soil column depth and representation of soil organic matter, *J.*
211 *Geophys. Res.* **113**, F02011 (2008).

212 11. S. C. Whalen, W. S. Reeburgh, Consumption of atmospheric methane by tundra soils, *Nature* **346**, 160–
213 162 (1990).

214 12. G. J. Luo, R. Kiese, B. Wolf, K. Butterbach-Bahl, Effects of soil temperature and moisture on methane
215 uptake and nitrous oxide emissions across three different ecosystem types, *Biogeosciences* **10**, 3205–3219
216 (2013).

217 13. B. Stackhouse *et al.*, Vertical gas fluxes, geochemical characteristics, and microbial community of
218 polygonal active layer and permafrost during progressive spring thaw, *Glob. Chang. Biol.* **in review**
219 (2013).

220 14. D. M. Degelmann, W. Borken, H. L. Drake, S. Kolb, Different atmospheric methane-oxidizing
221 communities in European beech and Norway spruce soils., *Appl. Environ. Microbiol.* **76**, 3228–3235
222 (2010).

223 15. C. Martineau *et al.*, Atmospheric methane oxidizers are present and active in Canadian high Arctic
224 soils, *Environ. Microbiol. Rep.* **in review** (2013).

225 16. T. G. Bárcena, K. W. Finster, J. C. Yde, Spatial Patterns of Soil Development, Methane Oxidation, and
226 Methanotrophic Diversity along a Receding Glacier Forefield, Southeast Greenland, *Arctic, Antarct. Alp.*
227 *Res.* **43**, 178–188 (2011).

228 17. P. Ricke *et al.*, First Genome Data from Uncultured Upland Soil Cluster Alpha Methanotrophs Provide
229 Further Evidence for a Close Phylogenetic Relationship to Methylocapsa acidiphila B2 and for High-

Affinity Methanotrophy Involving Particulate Methane Monooxygenase, *Appl. Environ. Microbiol.* **71**, 7472–7482 (2005).

18. M. Baani, W. Liesack, Two isozymes of particulate methane monooxygenase with different methane oxidation kinetics are found in Methylocystis sp. strain SC2, *Proc. Natl. Acad. Sci. USA* **105**, 10203–10208 (2008).

19. J. Benstead, G. M. King, H. G. Williams, Methanol promotes atmospheric methane oxidation by methanotrophic cultures and soils., *Appl. Environ. Microbiol.* **64**, 1091–1098 (1998).

20. R. Balasubramanian *et al.*, Oxidation of methane by a biological dicopper centre, *Nature* **465**, 115–119 (2010).

21. A. J. Paszczynski *et al.*, Proteomic and targeted qPCR analyses of subsurface microbial communities for presence of methane monooxygenase, *Biodegradation* **22**, 1045–1059 (2011).

22. J. C. Murrell, B. Gilbert, I. R. McDonald, Molecular biology and regulation of methane monooxygenase, *Arch. Microbiol.* **173**, 325–332 (2000).

23. I. R. McDonald, L. Bodrossy, Y. Chen, J. C. Murrell, Molecular ecology techniques for the study of aerobic methanotrophs., *Appl. Environ. Microbiol.* **74**, 1305–1315 (2008).

24. S. C. Whalen, W. S. Reeburgh, Moisture and temperature sensitivity of CH4 oxidation in boreal soils, *Soil Biol. Biochem.* **28**, 1271–1281 (1996).

25. S. C. Whalen, Biogeochemistry of methane exchange between natural wetlands and the atmosphere, *Environ. Eng. Sci.* **22**, 73–94 (2005).

26. M. S. Castro, P. A. Steudler, J. M. Melillo, J. D. Aber, R. D. Bowden, Factors controlling atmospheric methane consumption by temperate forest soils, *Global Biogeochem. Cycles* **9**, 1–10 (1995).

27. C. S. Sturtevant, W. C. Oechel, Spatial variation in landscape-level CO2 and CH4 fluxes from arctic coastal tundra: influence from vegetation, wetness, and the thaw lake cycle., *Glob. Chang. Biol.* **19**, 2853–2866 (2013).

28. C. A. Pickett-Heaps *et al.*, Magnitude and seasonality of wetland methane emissions from the Hudson Bay Lowlands (Canada), *Atmos. Chem. Phys.* **11**, 3773–3779 (2011).

29. S. Houweling, F. Dentener, J. Lelieveld, B. Walter, E. Dlugokencky, The modeling of tropospheric methane: How well can point measurements be reproduced by a global model., *J. Geophys. Res.* **105**, 8981–9002 (2000).

30. T. Sowers, Atmospheric methane isotope records covering the Holocene period, *Quat. Sci. Rev.* **29**, 213–221 (2010).

31. J. Maurer, Atlas of the Cryosphere (2007).

32. S. Kolb, The quest for atmospheric methane oxidizers in forest soils, *Environ. Microbiol. Rep.* **1**, 336–346 (2009).

33. M. Adachi, T. Ohtsuka, T. Nakatsubo, H. Koizumi, The methane flux along topographical gradients on a glacier foreland in the High Arctic, Ny-Ålesund, Svalbard, *Polar Biosci.* **20**, 131–139 (2006).

34. M. E. Brummell, R. E. Farrell, S. D. Siciliano, Greenhouse gas soil production and surface fluxes at a high arctic polar oasis, *Soil Biol. Biochem.* **52**, 1–12 (2012).

35. M. Mastepanov *et al.*, Large tundra methane burst during onset of freezing, *Nature* **456**, 628–631 (2008).

36. T. R. Christensen *et al.*, Trace gas exchange in a high-arctic valley 1. Variations in CO2 and CH4 flux between tundra vegetation types, *Glob. Biogeochemcial Cycles* **14**, 701–713 (2000).

37. S. Liebner *et al.*, Methane oxidation associated with submerged brown mosses reduces methane emissions from Siberian polygonal tundra, *J. Ecol.* **99**, 914–922 (2011).

38. T. Sachs, C. Wille, J. Boike, L. Kutzbach, Environmental controls on ecosystem-scale CH4 emission from polygonal tundra in the Lena River Delta, Siberia, *J. Geophys. Res.* **113**, G00A03 (2008).

39. K. Bäckstrand *et al.*, Annual carbon gas budget for a subarctic peatland, Northern Sweden, *Biogeosciences* **7**, 95–108 (2010).

40. J. Allan *et al.*, Methanogen Community Composition and Rates of Methane Production in Canadian High Arctic Permafrost Soils, *Environ. Microbiol. Rep.* **in review** (2013).

41. S. C. Whalen, W. S. Reeburgh, V. A. Barber, Oxidation of methane in boreal forest soils : a comparison of seven measures, *Biogeochemistry* **16**, 181–211 (1992).

42. P. Roslev, N. Iversen, K. Henriksen, Oxidation and assimilation of atmospheric methane by soil methane oxidizers., *Appl. Environ. Microbiol.* **63**, 874–880 (1997).

43. A. Rodionow, H. Flessa, O. Kazansky, G. Guggenberger, Organic matter composition and potential trace gas production of permafrost soils in the forest tundra in northern Siberia, *Geoderma* **135**, 49–62 (2006).

44. S. Liebner, D. Wagner, Abundance, distribution and potential activity of methane oxidizing bacteria in permafrost soils from the Lena Delta, Siberia., *Environ. Microbiol.* **9**, 107–117 (2007).

45. D. M. Degelmann, W. Borken, S. Kolb, Methane oxidation kinetics differ in European beech and Norway spruce soils, *Eur. J. Soil Sci.* **60**, 499–506 (2009).

46. C. Martineau, L. G. Whyte, C. W. Greer, Stable isotope probing analysis of the diversity and activity of methanotrophic bacteria in soils from the Canadian high Arctic, *Appl. Environ. Microbiol.* **76**, 5773–5784 (2010).

47. E. Yergeau, H. Hogues, L. G. Whyte, C. W. Greer, The functional potential of high Arctic permafrost revealed by metagenomic sequencing, qPCR and microarray analyses, *ISME J.* **4**, 1206–1214 (2010).

48. R. C. Wilhelm, T. D. Niederberger, C. Greer, L. G. Whyte, Microbial diversity of active layer and permafrost in an acidic wetland from the Canadian High Arctic, *Can. J. Microbiol.* **57**, 303–315 (2011).

49. I. Wartiainen, A. G. Hestnes, M. M. Svenning, Methanotrophic diversity in high arctic wetlands on the islands of Svalbard (Norway) — denaturing gradient gel electrophoresis analysis of soil DNA and enrichment cultures, *Can. J. Microbiol.* **612**, 602–612 (2003).

50. A. Tveit, R. Schwacke, M. M. Svenning, T. Urich, Organic carbon transformations in high-Arctic peat soils: key functions and microorganisms, *ISME J.* **7**, 1–13 (2012).

51. C. Graef, A. G. Hestnes, M. M. Svenning, P. Frenzel, The active methanotrophic community in a wetland from the High Arctic, *Environ. Microbiol. Rep.* **3**, 466–472 (2011).

52. S. Liebner, K. Rublack, T. Stuehrmann, D. Wagner, Diversity of Aerobic Methanotrophic Bacteria in a Permafrost Active Layer Soil of the Lena Delta, Siberia, *Microb. Ecol.* **57**, 25–35 (2009).

53. D. Wagner, A. Lipski, A. Embacher, A. Gattinger, Methane fluxes in permafrost habitats of the Lena Delta: effects of microbial community structure and organic matter quality, *Environ. Microbiol.* **7**, 1582–1592 (2005).

54. B. A. Barbier *et al.*, Methane-cycling communities in a permafrost-affected soil on Herschel Island, Western Canadian Arctic: active layer profiling of mcrA and pmoA genes., *FEMS Microb. Ecol.* **82**, 287–302 (2012).

55. S. Liebner, M. M. Svenning, Environmental transcription of mmoX by methane-oxidizing Proteobacteria in a Sub-arctic palsa peatland, *Appl. Environ. Microbiol.* **79**, 701–706 (2013).

56. R. Mackelprang *et al.*, Metagenomic analysis of a permafrost microbial community reveals a rapid response to thaw, *Nature* **480**, 368–371 (2011).

57. M. G. Kaliuzhnaia *et al.*, Methanotrophic communities in the soils of Russian northern taiga and subarctic tundra, *Mikrobiologiya* **71**, 264–271 (2002).

58. M. Pacheco-Oliver, I. R. McDonald, D. Groleau, J. C. Murrell, C. B. Miguez, Detection of methanotrophs with highly divergent pmoA genes from Arctic soils., *FEMS Microbiol. Lett.* **209**, 313–319 (2002).

59. J. M. Buttle, K. E. Fraser, Fluxes in a High Arctic Basin Wetland Snowmelt Hydrochemical during Spring, *Arctic, Antarct. Alp. Res.* **24**, 153–164 (1992).

60. C. J. Allan, S. Schiff, D. C. Pierson, M. Ecclestone, W. P. Adams, in *Proceedings of the National Student Conference on Northern Studies*, W. P. Adams, P. G. Johnson, Eds. (1985), pp. 239–252.

61. T. Vishnivetskaya *et al.*, Commercial DNA Extraction Kits Impact Observed Microbial Community Composition in Permafrost Samples, *FEMS Microb. Ecol.* .

62. F. Meyer *et al.*, The metagenomics RAST server - a public resource for the automatic phylogenetic and functional analysis of metagenomes, *BMC Bioinformatics* **9**, 386 (2008).

63. D. H. Parks, R. G. Beiko, Identifying biologically relevant differences between metagenomic communities., *Bioinformatics* **26**, 715–721 (2010).

64. L. Nazaries, J. C. Murrell, P. Millard, L. Baggs, B. K. Singh, Methane, microbes and models: fundamental understanding of the soil methane cycle for future predictions., *Environ. Microbiol.* **15**, 2395–2417 (2013).

65. T. Namiki, T. Hachiya, H. Tanaka, Y. Sakakibara, MetaVelvet: an extension of Velvet assembler to de novo metagenome assembly from short sequence reads, *Nucleic Acids Res.* **40**, e155 (2012).

66. B. Langmead, C. Trapnell, M. Pop, S. L. Salzberg, Ultrafast and memory-efficient alignment of short DNA sequences to the human genome., *Genome Biol.* **10**, R25 (2009).

67. K. Katoh, K. Kuma, H. Toh, T. Miyata, MAFFT version 5: improvement in accuracy of multiple sequence alignment., *Nucleic Acids Res.* **33**, 511–518 (2005).

68. D. Darriba, G. L. Taboada, R. Doallo, D. Posada, ProtTest 3: fast selection of best-fit models of protein evolution, *Bioinformatics* **27**, 1164–1165 (2011).

69. S. Q. Le, O. Gascuel, An improved general amino acid replacement matrix, *Mol. Biol. Evol.* **25**, 1307–1320 (2008).

70. A. Stamatakis, RAxML-VI-HPC: maximum likelihood-based phylogenetic analyses with thousands of taxa and mixed models, *Bioinformatics* **22**, 2688–2690 (2006).

71. A. Stamatakis, P. Hoover, J. Rougemont, A rapid bootstrap algorithm for the RAxML web servers, *Syst. Biol.* **57**, 758–771 (2008).

72. K. Chourey *et al.*, Direct cellular lysis/protein extraction protocol for soil metaproteomics, *J. Proteome Res.* **9**, 6615–6622 (2010).

73. S. D. Brown *et al.*, Molecular dynamics of the Shewanella oneidensis response to chromate stress, *Mol. Cell. Proteomics* **5**, 1054–1071 (2006).

353 74. N. C. Thompson, M R VerBerkmoes, K. Chourey, M. Shah, Dosage-dependent proteome response of
354 Shewanella oneidensis MR-1 to acute chromate challenge, *J. Proteome Res.* **6**, 1745–1757 (2006).

355 75. R. Sharma *et al.*, Coupling a detergent lysis/cleanup methodology with intact protein fractionation for
356 enhanced proteome characterization, *J. Proteome Res.* **11**, 6008–6018 (2012).

357 76. N. C. VerBerkmoes *et al.*, Shotgun metaproteomics of the human distal gut microbiota, *ISME J.* **3**, 179–
358 189 (2009).

359 77. J. K. Eng, A. L. McCormack, J. R. I. Yates, An approach to correlate tandem mass spectral data of
360 peptides with amino acid sequences in a protein database, *J. Am. Soc. MassSpectrometry* **5**, 976–989
361 (1994).

362 78. D. L. Tabb, W. H. McDonald, J. R. I. Yates, DTASelect and contrast: Tools for assembling and
363 comparing protein identifications from shotgun proteomics, *J. Proteome Res.* **1**, 21–26 (2002).

364 79. K. E. Taylor, R. J. Stouffer, G. A. Meehl, An overview of CMIP5 and the experiment design, *Bull. Am.*
365 *Meteorol. Soc.* **93**, 485–498 (2012).

366 80. D. Wunch *et al.*, The Total Carbon Column Observing Network, *Phil. Trans. R. Soc. A* **369**,
367 doi:10.1098/rsta.2010.0240 (2011).

368

369

Acknowledgments:

The project was supported by DOE grant DE-SC0004902 and NSF grant ARC-0909482.

The authors declare that they have no competing financial interests.

The data reported in this paper are available in the Supporting Online Materials and assembled contigs were uploaded to MG-RAST (ID: 4530050.3).

Fig. 1. CH_4 field fluxes in the northern circumpolar permafrost region. Sites that showed net CH_4 release are sources (numbers) whereas those showed atm CH_4 consumption are sinks (letters). The unit of CH_4 flux is mg CH_4-C m^{-2} day^{-1}. Circles with green outline indicate that the presence of atmMO is supported by microbial data. Information of soil characteristics is provided in Table S1. Background map was generated using the interactive tool "The Atlas of the Cryosphere" (*31*) available at the National Snow & Ice Data Center website (http://nsidc.org/data/atlas/).

Fig. 2. Temperature coefficients (Q_{10}) estimated from incubation experiments. All symbols mark the mid-point of the temperature range (denoted by the error bars) from which the Q_{10} was calculated. MWHC: Maximum water holding capacity. Please refer to Supplementary Notes for citations.

Fig. 3. Arrhenius relationship of CH_4 uptake and surface soil temperature at AHI. Expected log-CH4 fluxes (thick line) and 95% confident intervals (thin line) were estimated from best-fit linear regression analyses. The breakpoint temperature reads 3.588, as indicated by the dash line. Values of activation energy (Ea) and temperature coefficient (Q10) were derived from respective slopes. Results estimated from forest soils (parallel lines, (*26*)) are provided as a comparison. Please refer to Supplementary Notes for citations.

Table 1. Estimated monthly and annual CH_4 uptake fluxes at Axel Heiberg Island, Nunavut, Canada.

Supplementary Materials:

Notes

Materials and Methods

Fig. S1. Phylogenetic tree of *pmo*A genes constructed from deduced amino acid sequences (161 taxa and 171 aa). Highlighted is the gene recovered in this study. Sequences of ammonia-oxidizing monoxygenase (*amo*A) were used as the out-group. Clusters of atmospheric CH_4 oxidizers are annotated in reference to (*32*). Bootstrap values greater than 50% are shown as branch label. The scale bar represents a substitution rate of 0.2 changes per position.

Fig. S2. Phylogenetic tree of *pmo*B genes constructed from deduced amino acid sequences (69 taxa and 377 aa). Highlighted are the genes recovered in this study. Sequences of ammonia-oxidizing monoxygenase (*amo*B) were used as the out-group. Bootstrap values greater than 50% are shown as branch label. The scale bar represents a substitution rate of 0.2 changes per position.

Fig. S3. Phylogenetic tree of *pmoC* genes constructed from deduced amino acid sequences (82 taxa and 244 aa). Highlighted are the genes recovered in this study. Sequences of ammonia-oxidizing monoxygenase (*amo*C) were used as the out-group. Bootstrap values greater than 50% are shown as branch label. The scale bar represents a substitution rate of 0.2 changes per position.

Fig. S4. Predicted monthly air temperatures at Axel Heiberg Island, Nunavut, Canada.

Fig. S5. Regression model with segmented relationship(s).

Table S1. CH_4 field fluxes in the Northern Circumpolar permafrost region

Table S2. Methanotrophic taxa identified in near-surface cryosols (at 5 cm depth) in the intact core incubation experiment.

Table S3. Genes of methane monooxygenases and homologous enzymes identified in near-surface cryosols (at 5 cm depth) in the intact core incubation experiment.

Table S4. Methanotrophic proteins identified in near-surface cryosols (at 5 cm depth) in the intact core incubation experiment.

Table S5. Aerobic methanotrophs detected in Arctic permafrost-affected region

Table S6. CH_4 oxidation rates (mean±S.E.M.) estimated from microcosm experiments.

Table S7. Methanogenic taxa identified in near-surface cryosols (at 5 cm depth) in the intact core incubation experiment.

References (*32-80*)

Supplementary Materials

Notes:

References for data embedded in figures and tables

Fig. 1 and Table S1	(*11*, *12*, *28*, *33–41*)
Fig. 2	(*24*, *42–44*)
Fig. 3	(*11*, *12*, *26*, *37*, *41*, *45*)
Table S5	(*15*, *44*, *46–58*)

Responsibilities of the authors

T.C.O. conceived the study. B.T.S., N.C.S.M., P.B., G.L.-G., J.R. and L.G.W. extracted cores and performed field flux measurements and analyzed fluxes data. A.C.L., A.C., T.V. and S.M. performed metagenomic analysis. K.C. carried out the proteomic analysis of the crysols. K.C. and R.L.H analyzed the proteome data. M.C.Y.L. performed phylogenetic analysis. M.C.Y.L., B.T.S. and T.C.O. designed incubation experiments. B.T.S. carried out the intact core experiment and N.B. set up the microcosm experiment. C.R.O. and W.P. provided surface soil temperature record of 2013 at AHI. D.M.M. provided simulated temperature data. M.C.Y.L. performed analysis on thermal sensitivity and estimated annual fluxes. All authors discussed the results. M.C.Y.L. wrote the manuscript and all authors commented on the drafts.

449 **Materials and Methods:**

450 *Site description*

451 The study site is located at an upland polygonal terrain in proximity to the McGill
452 Arctic Research Station (MARS) at Expedition Fjord (79°24”57’N, 90°45”46’W), Axel
453 Heiberg Island (AHI), Nunavut, Canada. The average depth of the active layer varied
454 between 30 and 70 cm (field seasons 2011-2013) and the water table sat at 65 cm. The
455 mean soil temperatures in mid-summer (July 14, 2013) at both polygon interior and ice
456 wedge were 9±0.8°C at 5 cm depth and decreased to 3±1.4°C at 20 cm depth. The soil
457 temperature was measured by LiCOR thermistor (Maxim Integrated Products,
458 California).

459 The terrain was covered with vegetation such as Arctic grasses (e.g. *Puccinellia*
460 *arctica*, *Salix arctica*, *Polygonum viviparum*, *Dryas* sp., Saxifraga sp., *Papaver* sp.,
461 *Eriophorum* sp.) and lichens. Grasses were more abundant along the ice wedge troughs.
462 The polygon (16x16m) from which cryosols were collected for incubation and molecular
463 studies was sparsely vegetated but root materials were present to 15 cm depth (*13*). The
464 soil was previously described as a black acidic Gleysolic cryosol (*59*, *60*). Soil
465 characteristics and pore water chemistry has been analyzed by Stackhouse *et al*. (*13*).
466 Briefly, the cryosols were slightly acidic (pH 5.5 – 6). The top 10 cm of the active layer
467 had up to 6 wt% of organic carbon but was much lower (~1 wt%) from 10 cm down to
468 the permafrost table during summer. Total nitrogen did not vary with depth (0.1 wt%).

469

Field flux measurements

In situ CH_4 fluxes were measured in July 2011-2013 using a Picarro soil CO_2-CH_4 gas analyzer (Santa Clara, CA, USA) or Los Gatos Fast Methane Analyzer (Los Gatos Research Inc., Mountain View, CA).

Surface fluxes were measured in replicates using open-circuit dark chambers with continuous gas replacement from the air in 2011-2013 or closed-static chamber in 2013. For the open-circuit method, gas was continuously sampled (flow rate = 25 cm^3 min^{-1}) and analyzed at approximately 1 hz sample rate for CH_4, CO_2, H_2O, and $^{13}CO_2$, with alternating analysis periods of atmosphere and standard calibration gas. The flux chamber interior was continuously mixed with a small fan, and sample periods ranged from 45-600 min, with 45 min found to be the time needed to reach steady state concentration. The CH_4 uptake rates were calculated from the difference between initial atmospheric CH_4 concentration and the stabilized CH_4 concentration, with molar volume corrected for temperature using soil surface temperature and barometric pressure. For the closed-static method, the net loss of CH_4 was calculated by comparing the initial atmospheric CH_4 concentration and the final CH_4 concentration being measured at the end of a 4-minute duration. Subsurface CH_4 concentration was measured directly using gas sipper tubes installed into shallow boreholes at various depths and sealed into place with bentonite clay to prevent atmospheric contamination. Soil temperatures at corresponding depths were measured by LiCOR thermistor (Maxim Integrated Products, California).

491

492 *Abundance of methanotrophs and methanogens*

493 As part of the long-term intact core incubation experiment, 4 g of cryosols were
494 collected and processed as described in (*13*, *61*). Metagenome shotgun libraries of were
495 sequenced on an Illumina HiSeq 2000 platform. Results of 10 near-surface (at 5 cm
496 depth) cryosoal samples representing different time point (T=0, 1 week, 6 months and 12
497 months) were analyzed.

498 Raw data was processed through MG-RAST pipeline (*62*) which first
499 demultiplexed and removed sample identifier and then joined overlapping pair-end reads.
500 Low quality sequences, artificial duplicate sequences were removed as part of the quality
501 control (QC) pipeline. The number of post-QC reads per library averaged 1.7×10^7 with
502 an average size of 2.3 Gbp. Gene features were predicted and annotated by searching
503 against M5NR database and taxonomically classified to species level by "Best Hit
504 Classification" using the default values (Max. e-Value Cutoff=1e-5, Min. % Identity
505 Cutoff = 60% and Min. Alignment Length Cutoff = 15). The frequency data of these 10
506 libraries was exported from MG-RAST into STAMP (*63*). Hit abundance data was
507 normalized to the total sequences passing the QC pipeline. Only the methanotrophic and
508 methanogenic genera (as reviewed by (*64*)) with relative abundances > 0.001% were
509 considered. The relative abundance of individual genus was not statistically different at
510 the 0.05 level (ANOVA in STAMP) and therefore means (and standard deviations) of all
511 10 samples were reported.

Construction of pmo gene contigs

De novo co-assembly of raw sequences from 10 libraries (five 1-week and five 6-months thawed samples at 5 cm depth) were performed using MetaVelvet (*65*). Functional classifications were annotated separately via IMG/ER and MG-RAST using SEED Subsystem and GenBank using the default values (Max. e-Value Cutoff=1e-5, Min. % Identity Cutoff = 60% and Min. Alignment Length Cutoff = 15). Contigs identified as "methane monooxygenase" were searched for protein-coding genes because they may contain fragments of more than one gene. Phylogenetic affiliation of individual gene was queried against the NCBI non-redundant protein database using BlastX. Raw reads were mapped to each of the 10 contigs using Bowtie (*66*) to compute the relative abundance. Mean abundances (and standard deviations) of 10 samples were reported. Raw reads of five 1-week thawed samples (5 cm depth) to the representative *pmoCAB* operon of USCa recovered by bacterial artificial chromosome (BAC) cloning (*17*) were mapped to confirm the gene operon, *pmoCAB*, of the USCα genotype found at our study site.

Phylogenetic analyses of pmo gene contigs

Phylogenetic trees were constructed from deduced amino acid (aa) sequences for *pmo*A, *pmo*B and *pmo*C genes that encodes for α, β and γ subunit, respectively. All sequences had no frame-shift errors and no curation was applied.

Three datasets were created. The *pmoA* gene dataset contained (1) aa sequences of *pmoA* gene contigs from this study. One of *pmo*A genes was too short and thus omitted; (2) aa sequences of the best three BlastX matches; (3) aa sequences of all *pmoA* gene copies in published genomes of methanotrophs; (4) aa sequences of *pmoA* genes recovered from environmental studies of permafrost and atm CH_4-oxidizing sites; and (5) aa sequences of ammonia monooxygenases (*amoA* genes) that were used as the out-group. Sequences (2) – (5) were downloaded from NCBI (http://www.ncbi.nlm.nih.gov/). For some studies, aa sequences were not available and nt sequences were downloaded and translated. The dataset for *pmo*B and *pmoC* genes were created by the same approach.

For each dataset, sequences were aligned using MAFFT (*67*) included in freeware JalView package and manually edited using freeware Se-Al. Positions covered by more than half of the sequences were included while unaligned and ambiguous positions were trimed. Alignments of 161 taxa and 171 aa (*pmo*A genes), 69 taxa and 377 aa (*pmo*B) genes) and 82 and 244 aa (*pmo*C genes) were used for phylogenetic tree construction. ProtTest (v3.3) (*68*) selected the best-fit amino acid evolutionary model (LG+G and LG+G for *pmo*A and *pmo*B and LG+I+G for *pmo*C gene) (*69*) based on Bayesian Information Criterion. RAxML (v7.2.7 alpha) (*70*, *71*) was used to search for the best-scoring maximum likelihood (ML) tree with the selected matrix and empirically estimated base frequencies, and to perform a rapid bootstrap analysis of 100 iterations in single run. Tree editing was done using freeware FigTree (v1.3.1).

554 *Protein extraction and identification*

555 Three to 10 grams of frozen cryosol was mixed with SDS-based lysis buffer and
556 the slurry subjected to 15 min of boiling in a water bath with intermittent vortexing as
557 described earlier (*72*). The slurry was briefly cooled and centrifuged at 21000 g for 15
558 min and supernatant aliquoted to fresh tubes and amended with chilled 100% TCA to
559 final concentration of 25% followed by an overnight incubation at -20°C. The TCA-
560 precipitated proteins were collected via centrifugation at 21000 g for 15 min and the
561 resulting protein pellet was washed with chilled acetone (thrice), air dried and solubilized
562 in guanidine buffer [6M Guanidine HCl, 10 mM DTT in Tris CaCl2 buffer (10 mM Tris,
563 50 mM CaCl2, pH 7.8)] as described earlier (*72*). Total protein extracted from the
564 samples was estimated using the RC/DC protein estimation kit (Bio-Rad Laboratories,
565 Hercules, CA, USA) as per the manufacturer's protocol. The dissolved protein sample
566 was subjected to trypsin proteolysis for 16h at 37°C as described earlier (*72*, *73*). The
567 reaction was stopped by adding 10% formic acid to final concentration of 0.1% and kept
568 frozen at -80°C until MS analysis.

569 An aliquot of digested peptides was pressure loaded onto an in-house packed SCX
570 (Luna)-C18 (Aqua) column. The loaded sample column was subjected to an offline wash
571 with solvent A (5% acetonitrile, 0.1% formic acid in HPLC-grade water) for 5 min
572 followed by a gradient with 100% solvent B (70% acetonitrile, 0.1% formic acid in
573 HPLC-grade water) over 10 min. This step was repeated 3 times for a total offline wash
574 time of 45 min to desalt the column and get rid of any loosely attached contaminants. The
575 sample column was then connected to an in –house C18 packed Picofrit column (New

576 Objective, Woburn, MA) and the setup aligned on an Proxeon nanospray source in front
577 of an LTQ-Orbitrap (Thermo Fisher Scientific, San Jose, CA, USA) coupled to an
578 Ultimate 3000 HPLC system (Dionex, USA). Peptides were chromatographically
579 separated and analyzed via 24h Multi-Dimensional Protein Identification Technology
580 (MuDPIT) approach as described earlier (*74*, *75*) and the tandem mass spectra (MS/MS
581 scans) were acquired in a data dependent mode using Xcalibur software, V2.1.0 at
582 settings described previously (*76*). The raw spectra acquired by 12-step MS/MS runs
583 were searched via SEQUEST v.27 (*77*) against an artificially constructed pMMO
584 database using parameters described elsewhere (*74*, *75*). The output files were sorted and
585 filtered using DTASelect v. 1.9 (*78*) with Xcorr values of at least 1.8 (+1), 2.5 (+2), 3.5
586 (+3). Identification of at least two peptides per protein sequence was a set as criteria for
587 positive protein identifications. pMMO database included protein sequences translated
588 from MMO genes (1) co-assembled from DNA sequences of the 10 metagenomic
589 libraries stated above; (2) assembly of raw sequence reads annotated as "methane
590 monoxygenase"; and (3) mapping of raw sequence reads to methane monoxygenase
591 sequences obtained from GenBank. This database also included sequences of common
592 contaminants such as trypsin and keratin concatenated to the database.

593

594 *Microcosm incubation experiments*

595 Two sets of microcosms were set up to study the effect of temperature and water
596 saturation level on atm CH_4 oxidation rates. Prior to the experiment, 160 mL serum vials
597 were soaked in 10% HNO_3 overnight to remove trace metals, rinsed using distilled water

598 and combusted at 450°C for 8 hours. New butyl rubber stoppers were boiled in 0.1 N
599 NaOH for 45 minutes, soaked in distilled water for 8 hours and autoclaved.

600 A frozen core extracted in April 2011 (*13*) was dissected into sections for every
601 10 cm. The peripheral rim of 5 cm thick was discarded to remove any potential
602 contaminants from the core liner. The pristine cryosols were put into sterile Whirl-pak
603 bags and homogenized by hand. The 0-10 cm section was used in this experiment. The
604 original water content of the sample was determined to be 30.4±2.0 wt% by drying three
605 subsamples of 5 g at 50°C for four days. The cryosols were visibly fully saturated, thus
606 10 wt%, 20 wt% and 30 wt% were regarded as equivalent to water saturation levels of
607 33%, 66% and 100% respectively. Cryosols were preconditioned to attain the desired
608 water saturation by storing subsamples in a desiccator at 4°C.

609 Eight to ten grams (dry weight) of cryosol were put into vials and sealed with
610 treated butyl rubber stoppers and Al-crimps. Blank vials containing no soil were used to
611 track abiotic gas exchanges and minor instrumental drift. The headspace was flushed for
612 2-4 minutes with manufactured air (20% O_2, 80% N_2, 2.0 ppmv CH_4, and 400 ppmv
613 CO_2). Additional air was injected with a gas-tight glass syringe to over-pressurize the
614 vials to 1.5 atm. All treatments were run in triplicates. One set of 12 vials was incubated
615 at 4°C while another set was incubated at 10°C. Gas was sampled from the headspace at
616 T=0, twice for the first 2 weeks and weekly for another 2 weeks (period of incubation =
617 31 days). Analysis was performed on Picarro iCO2 (Model # G2101-I; Santa Clara, CA)
618 using the G2101-i coordinator. Instrumental sample dilution was accounted for by

multiplying a factor of 1.302 and the values were then corrected for dilution due to replacement.

Conversion between moles and ppm follows the ideal gas law:

$$10^{-6} mol = ppmv \times \frac{V}{RT}$$ where V is volume in L; R is gas constant, 0.0821 Latm $K^{-1}mol^{-1}$; T is temperature in K Eq. 1

Atm CH_4 oxidation follows first-order kinetics and hence rate constants, k, were calculated and used to estimate the oxidation rates at standardized CH_4 concentration of 1.813 ppmv and expressed in nmol (g of soil)$^{-1}$ day^{-1}.

Atm CH_4 oxidation rates obtained from microcosms experiments were scaled up to CH_4 fluxes to compare with the *in situ* flux measurements at the field. The following formula was used:

$$F = \frac{r \times FW}{d \times D}$$ where F is CH_4 flux in mg C $m^{-2}day^{-1}$; r is CH_4 oxidation rate in nmol $g^{-1}day^{-1}$; FW is formula weight of carbon, 12 g; d is density; D is depth in m Eq. 2

The density of 1.8×10^6 g m^{-3} (*13*) was used and the assumption of methanotrophic activity within the first 5 cm of active layer was taken. This may underestimate the flux values because field flux measurements indicated that atm CH_4 oxidation at AHI occurred down to 45 cm depth.

Temperature coefficients (Q_{10})

Q_{10} is used to measure the rate of change of a chemical or biological reaction as a consequent of temperate increase of 10°C. It is a factor calculated from the following equation:

$$Q_{10} = \left(\frac{R_2}{R_1}\right)^{\left(\frac{10}{T_2 - T_1}\right)}$$ where R_2 and R_1 are rates, in the same unit, measured respectively at T_2 and T_1, in the same unit; for $T_2 > T_1$ Eq. 3

Q_{10} values were computed for methanotrophy using (1) mean CH_4 oxidation rates obtained from microcosms for each treatment and corresponding incubation temperatures; and (2) mean CH_4 oxidation rates reported in the literature for which temperature data was available. The criterion that the temperature difference between T_2 and T_1 being larger than 5°C was to calculate Q_{10} values.

Arrhenius relationship between in situ CH_4 uptake flux and surface soil temperature

Fluxes measured by open-circuit chambers were used to determine the relationship whereas those measured by close-static chambers were not included. This was to eliminate the variation resulted from different collection methods (*41*). Natural logarithm of CH_4 uptake fluxes (y-axis) was plotted against 1000/temperature (x-axis) to create an Arrhenius plot, which showed potential change in the slope. The data was then analyzed using the "Segmented" R package (cran.r-project.org/web/packages/segmented/). Davies' test was used to determine whether the change in the slope was statistically significant. Given the result suggested a breakpoint

occurred at 3.588 (equivalent to 5.6°C; $p = 0.006$), function *segmented()* was used to estimate the breakpoint and the slopes (Results in Fig. S5).

Linear regression equations were fitted to data points below and above 5.6°C.

$$LN(F) = \frac{-E_a}{R}\left(\frac{1000}{T}\right) + LN(A) \quad \text{Eq. 4}$$

where F is CH_4 flux in mg C $m^{-2}day^{-1}$; E_a is activation energy in kJ mol^{-1}; R is gas constant, 8.314 J $K^{-1}mol^{-1}$; T is temperature, in K; density; A is pre-exponential factor

Q_{10} and active energy (E_a) of atm CH_4 oxidation were derived from Eq. 3 and Eq. 4 respectively. 95% confidence intervals were calculated for each slope.

For comparative purpose, other data were overlain on the plot (Fig. 4) which include: (1) CH_4 fluxes estimated from our microcosm experiments at 2.0 ppmv of CH_4; (2) CH_4 fluxes estimated from intact core thawing experiments (*13*); and (3) atm CH4 oxidation sites at lower latitudes.

Estimation of monthly and annual atm CH_4 uptake fluxes

Monthly air temperatures at AHI during 1990s and 2090s were simulated through the Climate Model Intercomparison Project (CMIP5) using 9 climate models (BCC-CSM1.1, CCSM4, CSIRO-Mk3.6.0, GFDL-ESM2M, GISS-E2-R, HadGEM2-AO, IPSL-CM5A-MR and NorESM1-M) (*79*). The 'high emissions scenario' assuming mitigation policies in action (RCP8.5) was used to project the climate change in 2090s. Monthly and annual atm CH_4 uptake were estimated for temperatures from each model with the following assumptions:

a) Atm CH_4 uptake occurs at ground temperatures above 0°C. Field measurements taken during initial thaw in 2013 when soil surface temperature slowly warmed from -2°C to 10°C, CH_4 uptake increased from undetectable to -0.24 mg CH_4-C m^{-2} day^{-1}). First detectable consumptive flux corresponded roughly to the time when soil surface temperature was consistently above freezing.

b) Atm CH_4 uptake fluxes increase with temperature following an Arrhenius relationship (Eq. 4) and at a faster rate below 5.6°C than that above 5.6°C.

The sum of monthly uptake fluxes multiplied by the number of days in the month equaled the mean annual uptake flux. Upper and lower 95% confidence intervals were regarded as maximum and minimum annual uptake fluxes. Multi-model means were obtained by taking average across all models.

Air temperatures at Eureka, Ellesmere Island, Nunavut, Canada (N80°00”03’, W86°00”25’; 112 km NE of AHI) were available for 2010 and 2011 through Total Carbon Column Observing Network (TCCON) (*80*). Temperature data (T) from late March to August 2011 was used. Missing data was filled by assuming progressive changes between two nearest data points. The data of 2010 tracked nicely that of 2011, thus the average temperature in Sept 2010 was used to substitute the missing data of Sept 2011. Mean daily temperatures were calculated by averaging multiple measurements on the day, which were then average to give monthly temperatures. The monthly and annual uptake fluxes were estimated as aforementioned. Eureka is located at a higher latitude where the temperature is slightly cooler than that at AHI. CH_4 uptake fluxes therefore

were also calculated for T+1°C and T+6°C which, respectively, are more representative for our study site and also to mimic severe summer warming which was not projected by climate models.

Table 1. Estimated monthly and annual CH_4 uptake fluxes at Axel Heiberg Island, Nunavut, Canada.

	Multi-model mean 1900-1999	Multi-model mean 2090-2099	T 2011	T+1°C	T+6°C 2100
Est. monthly flux ($\mu g\ CH_4\text{-}C\ m^{-2}\ month^{-1}$)					
Jan	0	0	NA	NA	NA
Feb	0	0	NA	NA	NA
Mar	0	0	NA	NA	NA
Apr	0	0	0	0	0
May	0	0	0	0	0
Jun	-8 (UCI: -25; LCI: -2)	-25 (UCI: -41; LCI: -15)	-82 (UCI: -100; LCI: -67)	-87 (UCI: -104; LCI: -73)	-117 (UCI: -172; LCI: -80)
Jul	-19 (UCI: -35; LCI: -10)	-32 (UCI: -51; LCI: -38)	-109 (UCI: -148; LCI -80)	-115 (UCI: -166; LCI: -80)	-154 (UCI: -301; LCI: -79)
Aug	-5 (UCI: -21; LCI: -1)	-18 (UCI: -34; LCI: -10)	-71 (UCI: -96; LCI: -53)	-76 (UCI: -97; LCI: -60)	-103 (UCI: -133; LCI: -79)
Sept	0	-5 (UCI: -22; LCI: 1)	0	0	0
Oct	0	0	NA	NA	NA
Nov	0	0	NA	NA	NA
Dec	0	0	NA	NA	NA
Est. annual flux ($mg\ CH_4\text{-}C\ m^{-2}\ year^{-1}$)					
	-0.4 (UCI: -0.9; LCI: -0.2)	-1.8 (UCI: -3.1; LCI: -1.6)	-8.0 (UCI: -10.5; LCI: -6.1)	-8.5 (UCI: -11.3; LCI: -6.5)	-11.5 (UCI: -18.6; LCI: -7.3)

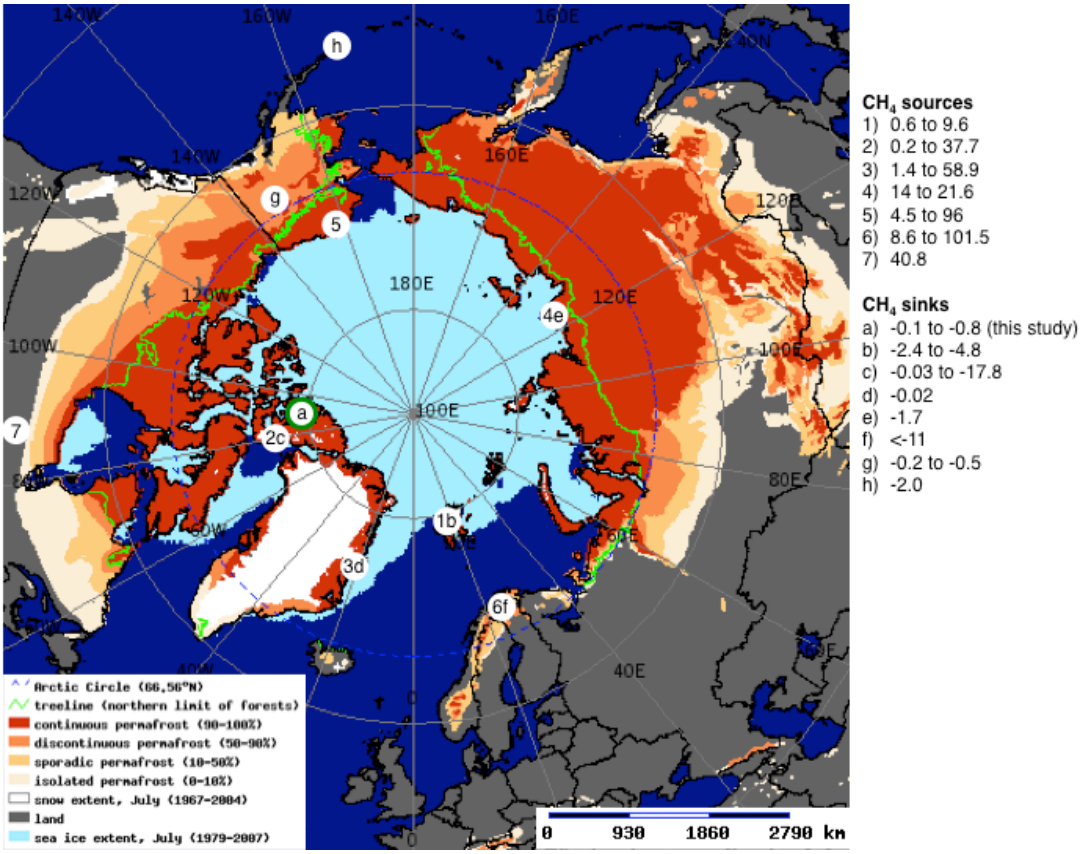

Fig. 1. CH_4 field fluxes in the northern circumpolar permafrost region. Sites that showed net CH_4 release are sources (numbers) whereas those showed atm CH_4 consumption are sinks (letters). The unit of CH_4 flux is mg CH_4-C m^{-2} day^{-1}. Circles with green outline indicate that the presence of atmMO is supported by microbial data. Information of soil characteristics is provided in Table S1. Background map was generated using the interactive tool "The Atlas of the Cryosphere" (*31*) available at the National Snow & Ice Data Center website (http://nsidc.org/data/atlas/).

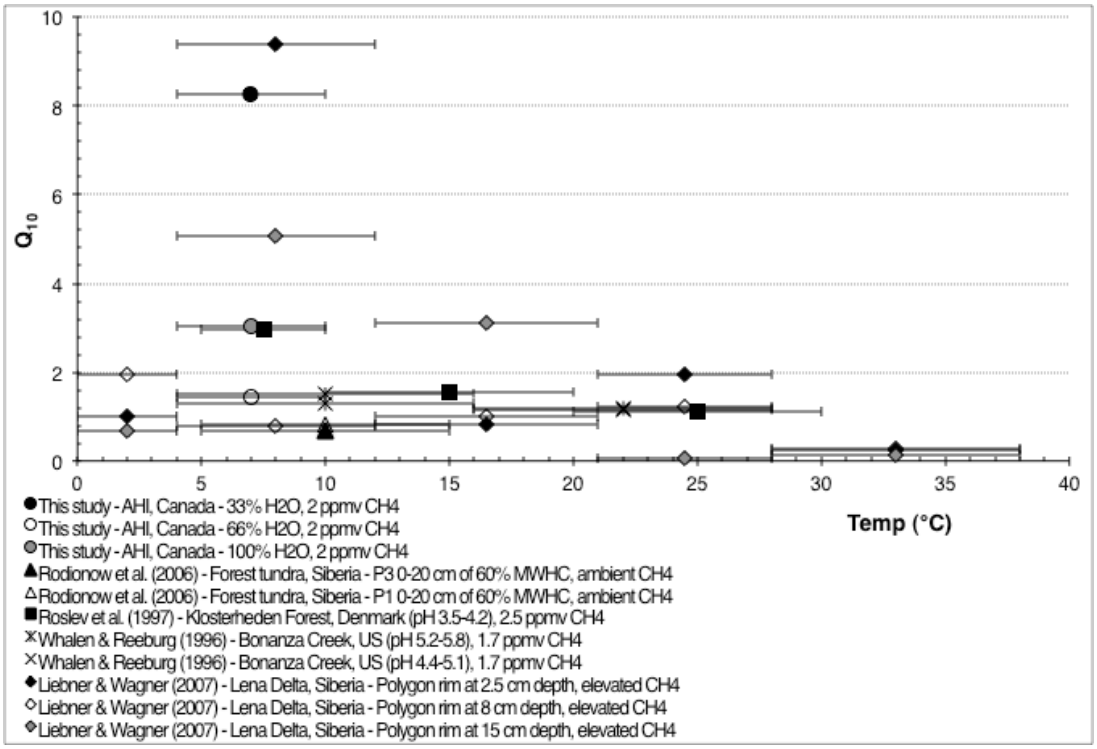

Fig. 2. Temperature coefficients (Q_{10}) estimated from incubation experiments. All symbols mark the mid-point of the temperature range (denoted by the error bars) from which the Q_{10} was calculated. MWHC: Maximum water holding capacity. Please refer to Supplementary Notes for citations.

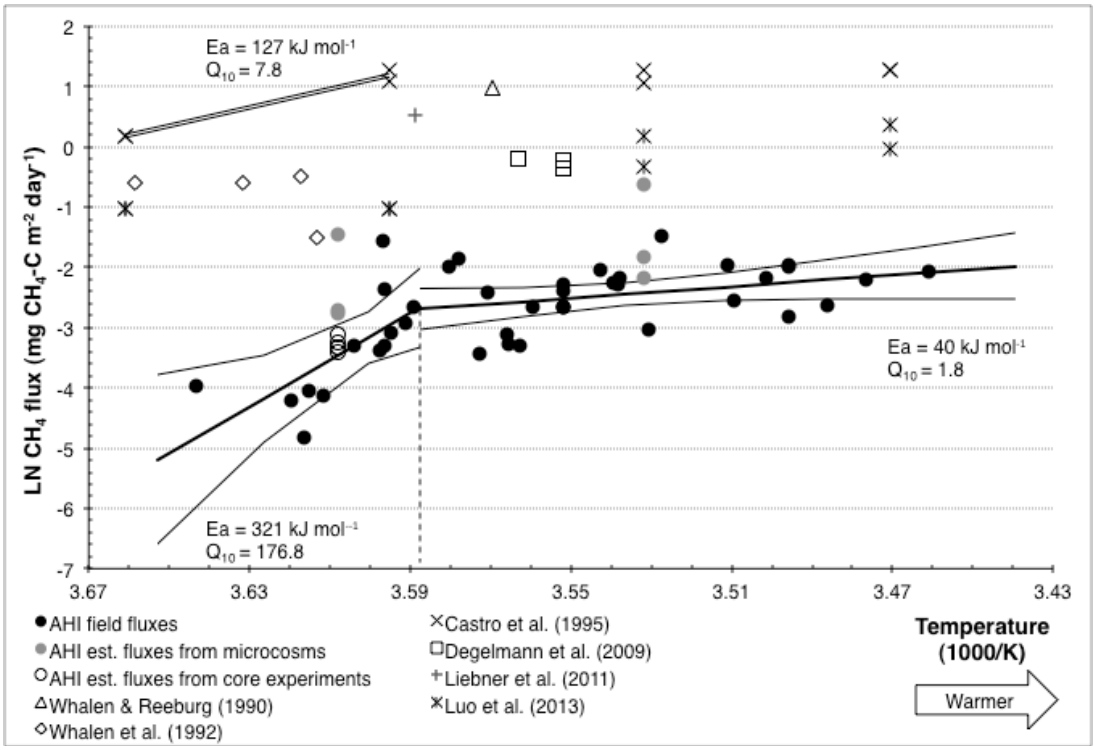

Fig. 3. Arrhenius relationship of CH_4 uptake and surface soil temperature at AHI. Expected log-CH4 fluxes (thick line) and 95% confident intervals (thin line) were estimated from best-fit linear regression analyses. The breakpoint temperature reads 3.588, as indicated by the dash line. Values of activation energy (Ea) and temperature coefficient (Q10) were derived from respective slopes. Results estimated from forest soils (parallel lines, (*26*)) are provided as a comparison. Please refer to Supplementary Notes for citations.

Fig. S1. Phylogenetic tree of pmoA genes constructed from deduced amino acid sequences (161 taxa and 171 aa). Highlighted is the gene recovered in this study. Sequences of ammonia-oxidizing monoxygenase (amoA) were used as the out-group. Clusters of atmospheric CH4 oxidizers are annotated in reference to (32). Bootstrap values greater than 50% are shown as branch label. The scale bar represents a substitution rate of 0.2 changes per position.

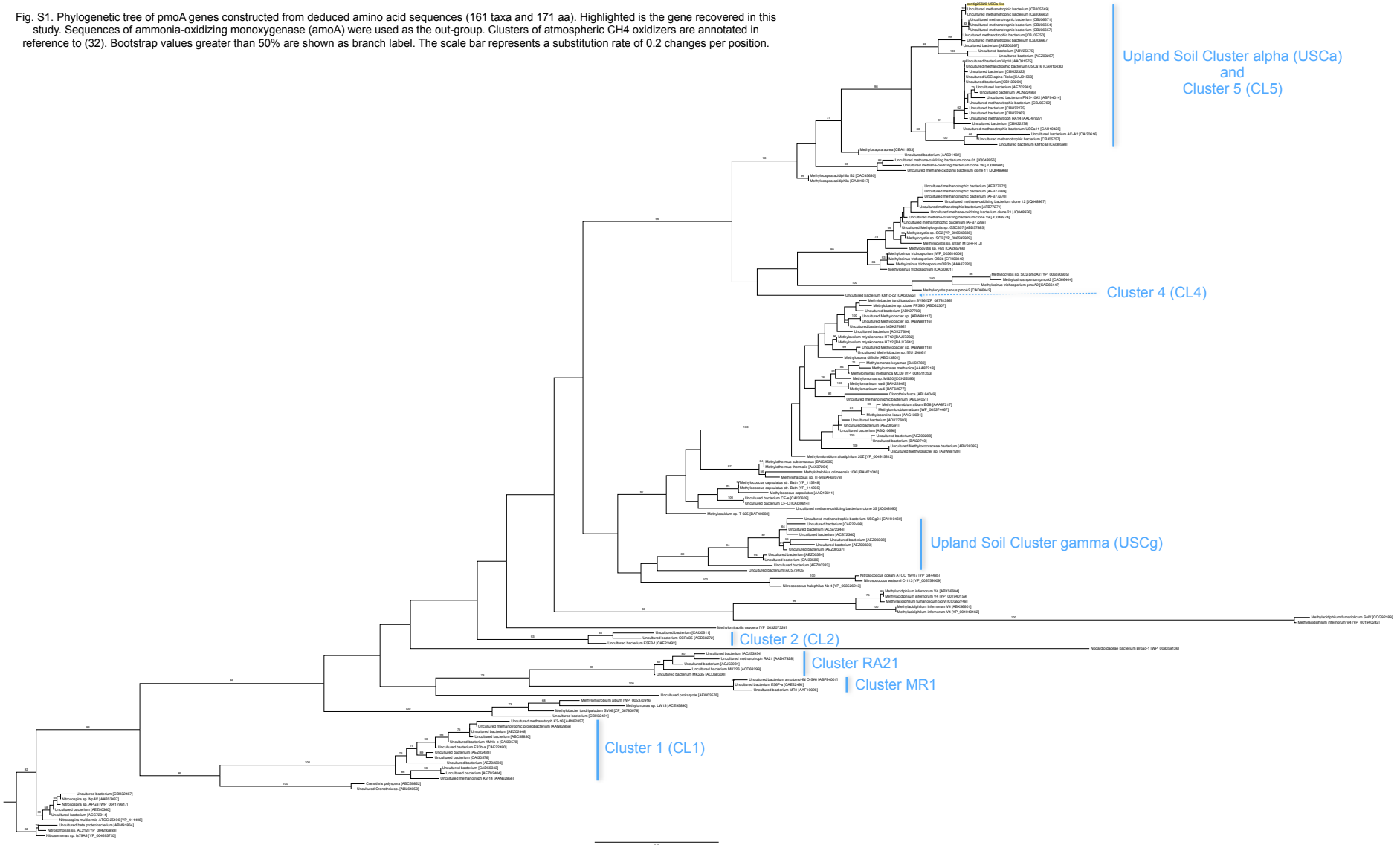

Fig. S2. Phylogenetic tree of pmoB genes constructed from deduced amino acid sequences (69 taxa and 377 aa). Highlighted are the genes recovered in this study. Sequences of ammonia-oxidizing monoxygenase (amoB) were used as the out-group. Bootstrap values greater than 50% are shown as branch label. The scale bar represents a substitution rate of 0.2 changes per position.

Fig. S3. Phylogenetic tree of pmoC genes constructed from deduced amino acid sequences (82 taxa and 244 aa). Highlighted are the genes recovered in this study. Sequences of ammonia-oxidizing monoxygenase (amoC) were used as the out-group. Bootstrap values greater than 50% are shown as branch label. The scale bar represents a substitution rate of 0.2 changes per position.

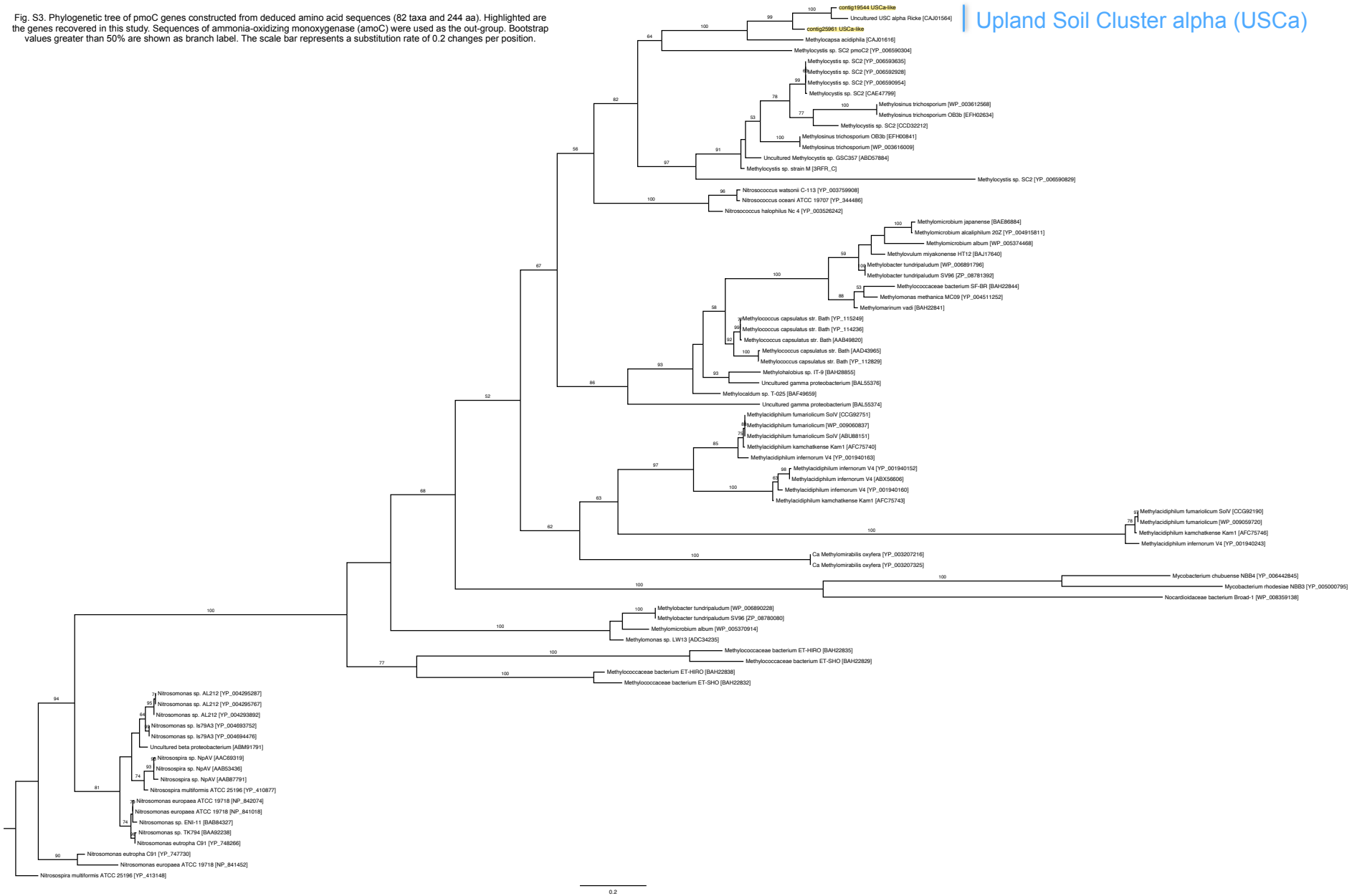

Fig. S4. Predicted monthly air temperatures at Axel Heiberg Island, Nunavut, Canada.

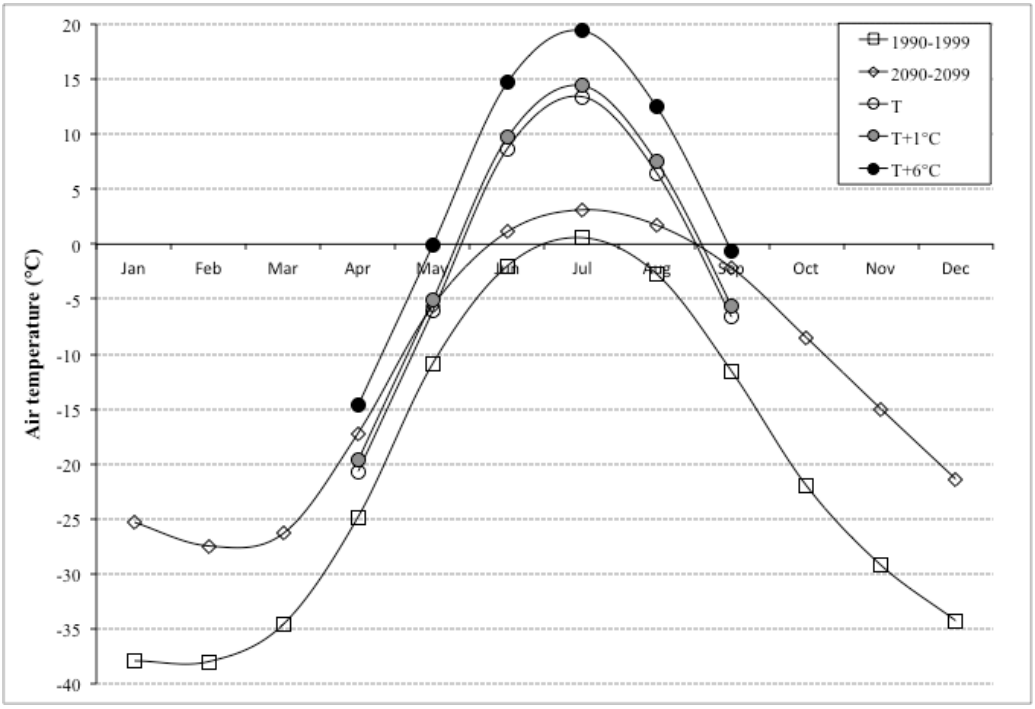

Fig. S5. Regression model with segmented relationship(s).

```
         ***Regression Model with Segmented Relationship(s)***

Call:
segmented.glm(obj = fit.glm, seg.Z = ~Temp, psi = 3.461)

Estimated Break-Point(s):
    Est.   St.Err
3.588000 0.008967

t value for the gap-variable(s) V:  0

Meaningful coefficients of the linear terms:
          Estimate Std. Error t value Pr(>|t|)
(Intercept)   14.749     11.015   1.339    0.189
Temp         -4.862      3.116  -1.560    0.127
U1.Temp     -33.765     10.657  -3.168       NA
(Dispersion parameter for gaussian family taken to be 0.2888783)

Null     deviance: 23.206  on 40  degrees of freedom
Residual deviance: 10.688  on 37  degrees of freedom
AIC: 69.232

Convergence attained in 2 iterations with relative change -9.87917e-16
```

Table S1. CH_4 field fluxes in the Northern Circumpolar permafrost region.

CH_4 source

	Site	Latitude	Longitude	Soil description	Vegetation	pH	Soil moisture (wt%	Bulk Soil C (wt%	Field season	Soil temp. (°C)[1]	CH_4 flux (mg CH_4-C m^{-2} day^{-1})	Reference	
1	Ny-Ålesund, Svalbard	79° N	12° E	Arctic tundra	Cardamine	7 – 7.5	50 – 75	10 – 12	2008 Aug	NA	0.6	Adachi et al. (2006)	33
1	Ny-Ålesund, Svalbard	79° N	12° E	Arctic tundra	Salix	6 – 7.7	50 – 100	4 – 25	2008 Aug	NA	9.6	Adachi et al. (2006)	33
1	Ny-Ålesund, Svalbard	79° N	12° E	Arctic tundra	Oxyria/*Luzula*	6.5 – 7.5	40 – 50	4 – 10	2008 Aug	NA	2.4	Adachi et al. (2006)	33
1	Ny-Ålesund, Svalbard	79° N	12° E	Arctic tundra	Bryophyte	6.8 – 7.3	40 – 50	4 – 12	2008 Aug	NA	7.2	Adachi et al. (2006)	33
2	Alexandra Fjord, Ellesmere Island, Canada	75°55' N	78°53' W	Barren	Cryptogam, herb barren	7.6 – 7.8	31 – 46	0.41 – 0.52	2009 late Jun – early Aug	NA	0.4	Brummell et al. (2012)	34
2	Alexandra Fjord, Ellesmere Island, Canada	75°55' N	78°53' W	Mountain	Noncarbonate mountain complex	6.5 – 7.0	47 – 55	0.35 – 0.53	2009 late Jun – early Aug	NA	0.3	Brummell et al. (2012)	34
2	Alexandra Fjord, Ellesmere Island, Canada	75°55' N	78°53' W	Prostrate	Prostrate dwarf-shrub, herb tundra	5.5 – 6.9	58 – 79	0.35 – 1.54	2009 late Jun – early Aug	NA	0.2	Brummell et al. (2012)	34
2	Alexandra Fjord, Ellesmere Island, Canada	75°55' N	78°53' W	Arctic wetland	Sedge/grass, moss wetland	6.4 – 6.6	75 – 92	0.05 – 6.85	2009 late Jun – early Aug	NA	37.7	Brummell et al. (2012)	34
3	Zackenberg Valley, Greenland	74°17'50" N	21°00'00" W	Arctic wetland	*Eriophorum scheuchzeri*, *Dupontia psilosantha*, *Arctagrostis latifolia*	NA	NA	NA	2007 late Jun – early Oct	-4 – 12°C @ 5 cm depth	58.9	Mastepanov et al. (2008)	35
3	Zackenberg Valley, Greenland	74°17'50" N	21°00'00" W	Arctic wetland	Hummocky fen (mosses, *Salix arctica* and *Polygonum viviparum*)	NA	NA	NA	2008 thaw season	15.5°C	7.6	Christensen et al. (2000)	36
3	Zackenberg Valley, Greenland	74°17'50" N	21°00'00" W	Arctic wetland	Continuous fen (*Eriophorum scheuchzeri* and *Dupontia psilosantha*)	NA	NA	NA	2009 thaw season	14.9°C	4.4	Christensen et al. (2000)	36
3	Zackenberg Valley, Greenland	74°17'50" N	21°00'00" W	Arctic wetland	Grassland (e.g. *Carex saxatilis*, *Eriophorum triste* and *Arctagrostis latifolia*)	NA	NA	NA	2010 thaw season	15.1°C	1.4	Christensen et al. (2000)	36
3	Zackenberg Valley, Greenland	74°17'50" N	21°00'00" W	Arctic wetland	*Salix arctica* snowbeds (*Salix arctica*, Alopecurus alpinus *and* Pedicularis lapponica)	NA	NA	NA	2011 thaw season	13.7°C	8.8	Christensen et al. (2000)	36
4	Lena River Delta, Siberia	72°22'197" N	126°28'951" E	Submerged polygon	*Scorpidium* moss	7.1	100	NA	2009 early Jul	4 – 7°C	21.6	Liebner et al. (2011)	37
4	Lena River Delta, Siberia	72°22'13" N	126°29'10" E	Polygonal tundra	Vegetated	NA	NA	NA	2006 Jun – Sept	NA	14	Sachs et al. (2008)	38
5	Near Barrow, Alaska	71° N	156° W	Wet meadow tundra	Graminoids (incl. *Arctophila fulva*, *Dupontia fisheri*, *Eriophorum* spp., *Carex aquatilis*), mosses (incl. *Sphagnum*, *Dicranum elongatum*), lichens and a few prostrate dwarf shrubs (*Salix* spp., *Cassiope teragona*)	NA	NA	NA	2011 Jun – Aug	3.3°C	4.5 to 96	Sturtevant & Oechel (2013)	27
6	Stordalen mire, Sweden	68°22' N	19°03' E	Intermediate thawed ground	*Sphagnum* spp. and *Carex* spp.	NA	NA	NA	2002 – 2007 (field measurements and gap-filling)	NA	8.6 to 21.1	Bäckstrand et al. (2010)	39
6	Stordalen mire, Sweden	68°22' N	19°03' E	Completely thawed ground	*Eriophorum angustifolium*	NA	NA	NA	2002 – 2007 (field measurements and gap-filling)	NA	66.5 to 101.5	Bäckstrand et al. (2010)	39
7	Hudson Bay lowlands	53° N	90° W	Boreal wetland		NA	NA	NA	Not applicable	NA	40.8	Picket-Heaps et al. (2011)	28

CH_4 sink

	Site	Latitude	Longitude	Soil description	Vegetation	pH	Soil moisture (wt%	Bulk Soil C (wt%	Field season	Soil temp. (°C)[1]	CH_4 flux (mg CH_4-C m^{-2} day^{-1})	Reference	
a	Expedition Fjord, Axel Heiberg Island, Canada	79°24'55" N	90°45'27" W	High-centered polygon	Lichen/mossess and sparse grass	NA	NA	NA	2011 Jul 15-16	15.8°C @ 5 cm depth	-0.18±0.04	Allan et al. (2013)	40
a	Expedition Fjord, Axel Heiberg Island, Canada	79°24'52" N	90°45'30" W	Arctic wetland	Cotton grass	NA	NA	NA	2011 Jul 15-16	17.9°C @ 5 cm depth	-0.16	Allan et al. (2013)	40
a	Expedition Fjord, Axel Heiberg Island, Canada	79°24'57" N	90°45'46" W	High-centered polygon	Sparse cover by grasses (e.g. *Puccinellia arctica*, *Salix arctica*, *Polygonum viviparum*, *Dryas* sp., *Saxifraga* sp., *Papaver* sp., *Eriophorum* sp.) and lichens	5.5 – 6	15 – 20	1 – 6	2011 Jul 9-14	12.4°C @ 5 cm depth	-0.07±0.01	This study (using open-circuit method)	
a	Expedition Fjord, Axel Heiberg Island, Canada	79°24'57" N	90°45'47" W	Ice wedge	Heavily cover by grasses (e.g. *Puccinellia arctica*, *Salix arctica*, *Polygonum viviparum*, *Dryas* sp., *Saxifraga* sp., *Papaver* sp., *Eriophorum* sp.)	5.5 – 6	15 – 20	1 – 6	2011 Jul 9-14	14.7°C @ 5 cm depth	-0.10±0.03	This study (using open-circuit method)	
a	Expedition Fjord, Axel Heiberg Island, Canada	79°24'57" N	90°45'46" W	High-centered polygon	Sparse cover by grasses (e.g. *Puccinellia arctica*, *Salix arctica*, *Polygonum viviparum*, *Dryas* sp., *Saxifraga* sp., *Papaver* sp., *Eriophorum* sp.) and lichens	5.5 – 6	15 – 20	1 – 6	2012 Jul 6-8	8.4°C @ 5 cm depth	-0.08±0.02	This study (using open-circuit method)	
a	Expedition Fjord, Axel Heiberg Island, Canada	79°24'57" N	90°45'46" W	High-centered polygon	Sparse cover by grasses (e.g. *Puccinellia arctica*, *Salix arctica*, *Polygonum viviparum*, *Dryas* sp., *Saxifraga* sp., *Papaver* sp., *Eriophorum* sp.) and lichens	5.5 – 6	15 – 20	1 – 6	2013 Jul 4-19	1.3 – 12.9°C @ 5 cm depth	-0.02±0.01 to -0.14±0.02	This study (using open-circuit method)	
a	Expedition Fjord, Axel Heiberg Island, Canada	79°24'57" N	90°45'47" W	High-centered polygon	Sparse cover by grasses (e.g. *Puccinellia arctica*, *Salix arctica*, *Polygonum viviparum*, *Dryas* sp., *Saxifraga* sp., *Papaver* sp., *Eriophorum* sp.) and lichens	5.5 – 6	15 – 20	1 – 6	2013 mid Jul	9.2°C @ 5 cm depth	-0.84±0.18	This study (using closed static method)	
b	Ny-Ålesund, Svalbard	79° N	12° E	Arctic tundra	*Salix*	6 – 7.7	50 – 100	4 – 25	2008 Aug	NA	-2.4	Adachi et al. (2006)	33
b	Ny-Ålesund, Svalbard	79° N	12° E	Arctic tundra	*Oxyria*/*Luzula*	6.5 – 7.5	40 – 50	4 – 10	2008 Aug	NA	-3.6	Adachi et al. (2006)	33
b	Ny-Ålesund, Svalbard	79° N	12° E	Arctic tundra	Bryophyte	6.8 – 7.3	40 – 50	4 – 12	2008 Aug	NA	-4.8	Adachi et al. (2006)	33
c	Alexandra Fjord, Ellesmere Island, Canada	75°55' N	78°53' W	Hemiprostrate	Prostrate/hemiprostrate dwarf-shrub	6.3 – 7.0	54 – 75	0.26 – 0.52	2009 late Jun – early Aug	NA	-0.03	Brummell et al. (2012)	34
c	Alexandra Fjord, Ellesmere Island, Canada	75°55' N	78°53' W	Sedge/dwraft-shrub	Nontussock sedge, dwarf-shrub, moss tundra	5.2 – 5.8	43 – 51	1.16 – 4.17	2010 late Jun – early Aug	NA	-0.1	Brummell et al. (2012)	34
c	Alexandra Fjord, Ellesmere Island, Canada	75°55' N	78°53' W	Arctic wetland	Sedge/grass, moss wetland	6.4 – 6.6	75 – 92	0.05 – 6.85	2011 late Jun – early Aug	NA	-17.8	Brummell et al. (2012)	34
d	Zackenberg Valley, Greenland	74°17'50" N	21°00'00" W	Arctic wetland	*Cassiope* heaths (*Cassiope tetragona* and *Vaccinium uliginosum*)	NA	NA	NA	2007 thaw season	16.1°C	-0.02	Christensen et al. (2000)	36
e	Lena River Delta, Siberia	72°22'13" N	126°29'10" E	Submerged polygon	*Scorpidium* moss	7.1	100	NA	2009 early Jul	4 – 7°C	-1.7	Liebner et al. (2011)	37
f	Stordalen mire, Sweden	68°22' N	19°03' E	Drained palsa areas	Woody herbaceous vegetation	NA	NA	NA	2002 – 2007 (field measurements and gap-filling)	-20 – 20°C[2]	<-9	Bäckstrand et al. (2010)	39
f	Stordalen mire, Sweden	68°22' N	19°03' E	Intermediate thawed ground	*Sphagnum* spp. and *Carex* spp.	NA	NA	NA	2002 – 2007 (field measurements and gap-filling)	-20 – 20°C[2]	<-11	Bäckstrand et al. (2010)	39
g	Bonanza Creek, Alaska, USA	64°45' N	148°18' W	Upland soils	north-facing black spruce	5	491	91	1990 Oct	0.2°C @ 10 cm depth	-0.41	Whalen et al. (1992)	41
g	Bonanza Creek, Alaska, USA	64°45' N	148°18' W	Upland soils	south-facing aspen (*Populus tremuloides*)	6.4	56	16	1990 Oct	3.6°C @ 10 cm depth	-0.17	Whalen et al. (1992)	41
g	Bonanza Creek, Alaska, USA	64°45' N	148°18' W	Upland soils	north-facing birch (*Betula papyrifera*)	5.9	69	24	1990 Oct	3.3°C @ 10 cm depth	-0.47	Whalen et al. (1992)	41
g	Bonanza Creek, Alaska, USA	64°45' N	148°18' W	Upland soils	south-facing white spruce (*Picea glauca*)	4.9	139	50	1990 Oct	2.2°C @ 10 cm depth	-0.41	Whalen et al. (1992)	41
h	Unalaska Island, Aleutian Islands	53° N	167° E	Moist tundra meadow	Mosses, liches, cottongrasses (*Eriophorum* sp.), low-lying ferns and dwarf shrubs (*Vaccinium* sp.)	NA	>100	16 – 38	1987 Oct	7°C	-2.03	Whalen & Reeburg (1990)	11

Note:
[1] ambient temperature unless specified
[2] Temperature range in year 2004
NA: Not available

Table S2. Methanotrophic taxa identified in near-surface cryosols (at 5 cm depth) in the intact core incubation experiment.

Class/Phylum	Family	Genus[1]	Dominant Species	Mean % abundance > 0.001% (± std)[3]	Methanotrophy/Type of Intracytoplasmic membrane (ICM)	Formaldehyde Assimilation Pathway	Type of MMO[4]
α-Proteobacteria	Beijerinckiaceae	*Methylocapsa*	*Methylocapsa acidiphila*[2]	0.0046 (±0.0024)	Facultative/Type II	Serine	pMMO only
α-Proteobacteria	Beijerinckiaceae	*Methylocella*	*Methylocella silvestis*	0.2930 (±0.1124)	Facultative/Type II	Serine	sMMO only
α-Proteobacteria	Methylocystaceae	*Methylocystis*	*Methylocystis* sp. ATCC 49242	0.0921 (±0.0282)	Obligate/Type II	Serine	pMMO & sMMO
α-Proteobacteria	Methylocystaceae	*Methylosinus*	*Methylosinus trichosporum*	0.0966 (±0.0309)	Obligate/Type II	Serine	pMMO & sMMO
				Subtotal = 0.49%			
γ-Proteobacteria	Methylococcaceae	*Methylobacter*	*Methylobacter tundripaludum*	0.0446 (±0.0118)	Obligate/Type I	Ribulose monophosphate (RuMP)	pMMO & sMMO
γ-Proteobacteria	Methylococcaceae	*Methylococcus*	*Methylococcus capsulatus*	0.0706 (±0.0191)	Obligate/Type I	Ribulose monophosphate (RuMP)	pMMO & sMMO
				Subtotal = 0.12%			
Verrucomicrobia	Methylacidiphilaceae	*Methylacidiphilum*	*Methylacidiphilum infernorum*	0.0887 (±0.0200)	Obligate/No ICM	Serine variant	pMMO only
				Total =0.69%			

Notes:

[1]Genera not detected: *Clonothrix*, *Crenothrix*, *Methylohalobius*, *Methylosoma*, *Methylothermus*, *Methylosphaera*, *Methylomarinum*, *Methylocaldum* and *Methylogaea*.

[2]The closest related isolate to atm CH4-oxidizing bacterium Upland Soil Cluster alpha (USCα).

[3]Mean abundance of 16 cryosol samples collected at different time during the course of incubation (T=0, 1 week, 6 months and 12 months).

[4]MMO: Methane monooxygenase; pMMO: particulate MMO; sMMO: soluble MMO

Table S3. Genes of methane monooxygenases and homologous enzymes identified in near-surface cryosols (at 5 cm depth) in the intact core incubation experiment.

De Novo Assembly ID	Size (bp)	Mean % abundance (± std)[1]	Putative gene	Closest protein match (BlastX)				
				Accesion no.	Taxon	Protein superfamily	Enzyme Encoded	% of identity
contig25620	1117	0.00015 (±0.00014)	*pmo*A	CAJ01563	Upland soil cluster alpha (USCalpha)	Pmo/Amo	α subunit of particulate methane monoxygenase (27-kDa) contains active site	87
contig19544	1301	0.00015 (±0.00012)	*pmo*C	CAJ01564	Upland soil cluster alpha (USCalpha)	Pmo/Amo	γ subunit of particulate methane monoxygenase	85
contig25961	1116	0.00029 (± 0.00033)	*pmo*A	CAJ01564	Upland soil cluster alpha (USCalpha)	Pmo/Amo	α subunit of particulate methane monoxygenase (27-kDa) contains active site	73
			*pmo*C	CAJ01565	Upland soil cluster alpha (USCalpha)	Pmo/Amo	γ subunit of particulate methane monoxygenase	86
contig60426	646	0.00005 (± 0.00003)	*pmo*B	CAJ01562	Upland soil cluster alpha (USCalpha)	Pmo/Amo	β subunit of particulate methane monoxygense (45-kDa)	70
contig78492	528	0.00003 (± 0.00003)	*pmo*B	CAJ01562	Upland soil cluster alpha (USCalpha)	Pmo/Amo	β subunit of particulate methane monoxygense (45-kDa)	85
contig20276	1272	0.00013 (± 0.00009)	*pmo*B	CAJ01562	Upland soil cluster alpha (USCalpha)	Pmo/Amo	β subunit of particulate methane monoxygense (45-kDa)	84
			Unknown	CAJ01561	Upland soil cluster alpha (USCalpha)		Conserved hypothetical protein	74
contig01417	4093	0.00039 (± 0.00033)	*amo*C	YP_006863929	Candidatus Nitrososphaera gargensis Ga9.2	Pmo/Amo	Subunit C of ammonia monooxygenase/methane monooxygenase	95
			*amo*A	AEQ03735	Uncultured crenarchaeote	Pmo/Amo	Subunit A of ammonium monooxygenase	99
contig08394	1973	0.00011 (± 0.00009)	*pmo* homolog	YP_001239622	Bradyrhizobium sp. BTAi1	Ferritin-like	α subunit of methane/phenol/toluene monooxygenase	97
contig62491	620	0.00006 (± 0.00002)	*pmo* homolog	YP_481616	Frankia sp. CcI3	Ferritin-like	Methane monooxygenase	83
contig61701	655	0.00012 (± 0.00003)	*pmo* homolog	YP_004330745	Pseudonocardia dioxanivorans CB1190	Ferritin-like	Methane monooxygenase	96
contig61059	630	0.00006 (± 0.00004)	*pmo* homolog	YP_005283808	Gordonia polyisoprenivorans VH2	Ferritin-like	Small subunit of putative phenol and propane monooxygenase	68
contig46385	636	0.00006 (± 0.00003)	*pmo* homolog	WP_010242492	Pseudonocardia sp. P1	Ferritin-like	Methane monoxygenase	68
contig56456	674	0.00005 (± 0.00003)	*pmo* homolog	WP_016880985	Rhodococcus sp. DK17	Ferritin-like	Methane monoxygenase	88

Notes:
[1]Mean abundance of 10 cryosol samples collected at different time during the course of incubation (T=1 week and 6 months).

Table S4. Methanotrophic proteins identified in near-surface cryosols (at 5 cm depth) in the intact core incubation experiment.

Sample	Locus	Sequence Count	Spectrum Count	Sequence Coverage	Protein Length	Adjusted NSAF*	Descriptive Name	MolWt (Daltons)	pI	XCorr	DeltCN	ObsM+H+	CalcM+H+	Ion%	Peptide Count	Sequence	Charge
Core A15, 1wk thaw	pMMOJGIMGRASTw1Acontig00008	2	2	0.347	75	22.8	pmoB [unculturedbacterium]	7873	5.2	4.54	0.76	1613.8099	1614.7526	70.00%	1	R.GLSLSDNSPIAPGETR.D	2
	pMMOw1w26Acontig00005	2	2	0.347	75	22.8	pmoB [unculturedbacterium]	7873	5.2	2.60	0.51	1086.4727	1088.2059	61.10%	1	R.DVAVTIQDAR.W	2
Core A15, 1wk thaw	fig|543016.3.peg.43	2	2	0.109	247	6.9	[Methylocapsa USClike uncultured] [Particulate methane monooxygenase B-subunit (EC 1.14.13.25)]	27489	9.6	3.51	0.72	1840.9594	1842.0563	65.60%	1	R.NIQALENEVDSGPITIK.Y	2
	pmoB_contig00023	2	2	0.065	413	4.1	manually translated USCalphalikepMMO	45464	7.1	3.22	0.64	1077.5647	1078.2133	94.40%	1	R.IGEFNTAGLR.F	2
Core A7, 12 month thaw	fig|543016.3.peg.43	2	4	0.085	247	18.3	[Methylocapsa USClike uncultured] [Particulate methane monooxygenase B-subunit (EC 1.14.13.25)]	27489	9.6	3.26	0.69	1077.5636	1078.2133	94.40%	3	R.IGEFNTAGLR.F	2
	pmoB_contig00023	2	4	0.051	413	10.9	manually translated USCalphalikepMMO	45464	7.1	2.67	0.64	1353.6624	1354.5022	80.00%	1	K.VEYPDYLLADR.G	2
Core A7, 12 month thaw	gi|83308654|emb|CAJ01562.1|	2	4	0.047	427	10.6	pmoB [Uncultured USCa Ricke]	47044	8.5	3.26	0.69	1077.5636	1078.2133	94.40%	3	R.IGEFNTAGLR.F	2

Notes:
NSAF: Normalized Spectral abundance factor
* Adjusted NSAF values: NSAF values multiplied by 1000000.

Table S5. Aerobic methanotrophs detected in Arctic permafrost-affected region

				46	46	47	47	48	15	15	15	this study	this study	49	50	50	51	52	52	53	44	54	55	56	57	58	58	58
				Martineau et al. (2010)	Martineau et al. (2010)	Yergeau et al. (2010)	Yergeau et al. (2010)	Wilhelm et al. (2011)	Martineau et al. (2013)	Martineau et al. (2013)	Martineau et al. (2013)			Wartiainen et al. (2003)	Tveit et al. (2013)	Tveit et al. (2013)	Graef et al. (2011)	Liebner et al. (2009)	Liebner et al. (2009)	Wagner et al. (2005)	Liebner et al. (2007)	Barbier et al. (2012)	Liebner et al. (2013)	Mackelprang et al. (2011)	Kaliuzhnaia et al. (2002)	Pacheco-Oliver et al. (2002)	Pacheco-Oliver et al. (2002)	Pacheco-Oliver et al. (2002)
			Location	Eureka, Ellesmere Island, Canadian high Arctic	Eureka, Ellesmere Island, Canadian high Arctic	Eureka, Ellesmere Island, Canadian high Arctic	Eureka, Ellesmere Island, Canadian high Arctic	Expedition Fjord, Axel Heiberg Island, Canadian high Arctic	Expedition Fjord, Axel Heiberg Island, Canadian high Arctic	Expedition Fjord, Axel Heiberg Island, Canadian high Arctic	Expedition Fjord, Axel Heiberg Island, Canadian high Arctic	Expedition Fjord, Axel Heiberg Island, Canadian high Arctic	Expedition Fjord, Axel Heiberg Island, Canadian high Arctic	Spitsbergen, Svalbard, Norway	Ny – Ålesund, Svalbard, Norway	Ny – Ålesund, Svalbard, Norway	Spitsbergen, Svalbard, Norway	Smoylov Island, the Lena Delta, Siberia	Smoylov Island, the Lena Delta, Siberia	Samoylov Island, the Lena Delta, Siberia	Samoylov Island, the Lena Delta, Siberia	Drained Lake', Herschel Island, Candaian Arctic	Norway	Hess Creek, Alaska, US	Russia	Kuujjuaq, Northern Quebec, Canada	Kuujjuaq, Northern Quebec, Canada	Kuujjuaq, Northern Quebec, Canada
			Lat, Long	80.000N, 85.839W	80.000N, 85.839W	80.000N, 85.839W	80.000N, 85.839W	79.433N, 90.766W	79.433N, 90.766W	79.433N, 90.766W	79.433N, 90.766W	79.415N, 90.757W	79.415N, 90.757W	78.933N, 11.883E and 78.250N, 15.5000E	78.926N, 11.944E and 78.933N, 11.818E	78.926N, 11.944E and 78.933N, 11.818E	78.917N, 11.933E	72.367N, 126.467E	72.367N, 126.467E	72.367N, 126.467E	72.367N, 126.467E	69.729N, 138.957W	69.694N, 29.383E	65.670N, 149.077W	NA	NA	NA	NA
			Soil description	Wet tundra	Wet tundra	Tundra	Tundra	Wetland	Acidic	Upland tundra	Wet meadow	High-centered polygon	High-centered polygon	Wetland	Peat bog	Peat bog	Wetland	Rim of low-centered polygon	Rim of low-centered polygon	Rim of low-centered polygon	Rim of low-centered polygon	Low-centered polygon	Degrading palsa	Peat soil	Subarctic tundra	Peat-like tundra (K3)	Peat-like tundra (K3)	Peat-like tundra (K3)
			Vegetation cover	NA	NA	NA	NA	NA	NA	NA	NA	Vegetated	Vegetated	Vegetated	Vegetated	Vegetated	Vegetated	NA	NA	Vegetated	NA	Vegetated	Vegetated	Vegetated	NA	NA	NA	NA
			Depth below surface (cm)	0 – 10	0 – 10	Surface	Surface	14 – 19	0 – 15	0 – 15	0 – 15	0 – 5	0 – 5	0 – 10	0 – 10	0 – 10	0 – 6	41436	41436	0 – 20	0 – 18	0 – 20	0 – 10	Active layer	41409	15 – 30	15 – 30	15 – 30
			Soil pH	6.7 – 7.1	6.7 – 7.1	7.9	7.9	4.48	4.8	6.4	6	5.5	5.5	5.0 – 6.7	5.2 – 5.8	5.2 – 5.8	NA	6.5	6.5	7.9	NA	5.2 – 5.6	4.2	6.48	NA	8.35	8.35	8.35
			Soil water content (wt%)	16 – 23	16 – 23	12.7	12.7	29.6	NA	NA	NA	15 – 20	15 – 20	75 – 90	70 – 90	70 – 90	NA	NA	NA	26.2 – 30.1	15.7 – 26.2	77 – 79	NA	82	NA	14.1	14.1	14.1
			Soil organic content (wt%)	3.80 – 5.60	3.80 – 5.60	3	3	0.98	NA	NA	NA	41279	41279	24 – 87	90 – 91	90 – 91	NA	2.1	2.1	2.1 – 2.4	2.1 – 3	23 – 28	NA	40	NA	9.43	9.43	9.43
			Incubation condition of soil being studied (if applicable)	Incubated soils at 4°C and RT in NMS medium with >8,000 ppmv CH_4	Incubated soils at 4°C and RT in NMS medium with >8,000 ppmv CH_4	NA	NA	NA	Incubated soils at 10°C 10 and 1000 ppmv CH_4	Incubated soils at 10°C 10 and 1000 ppmv CH_4	Incubated soils at 10°C 10 and 1000 ppmv CH_4	Incubated at 4°C with 2 ppmv CH4 for 1 – 26 weeks	Incubated at 4°C with 2 ppmv CH4 for 1 – 26 weeks	NA	NA	NA	Incubated at 15C with 10,000 and 50,000 ppmv of $^{13}CH_4$	NA	NA	NA	NA	NA	NA	Incubated soils at 5°C for 1 week with 20 ppmv CH_4 (trapped in frozen soils)	NA	NA	NA	NA
			Molecular method^	PCR-DGGE	PCR-DGGE	Meta-genomics	qPCR	PCR-DGGE	PCR-Cloning and Microarray	PCR-Cloning and Microarray	PCR-Cloning and Microarray	Meta-genomics	Meta-genomics	PCR-DGGE	Meta-transcriptomics	Meta-transcriptomics	PCR-Cloning	PCR-DGGE	PCR-DGGE	GC/MS	FISH	PCR-Cloning and TRFLP	PCR-Cloning	PCR	PCR	PCR-Cloning	PCR-Cloning	PCR-Cloning
			Biomarker	16S rDNA (universal)	pmoA	all genes (but no pmoA)	16S rDNA (methanotroph-specific)	16S rDNA (universal)	pmoA	pmoA	pmoA/ amoA	pmo	All raw sequences	16S rDNA (methanotroph-specific)	16S rRNA	pmoA	16S rRNA (universal)	16S rDNA (methanotroph-specific)	pmoA	PFLA	16S rDNA (methanotroph-specific)	pmoA	pmoA (no transcripts and no mmoX)	16S rDNA (methanotroph-specific)	16S rDNA (methanotroph-specific)	pmoA	mmoX	16S rRNA (methanotroph-specific)
Phylum	**Class**	**Family**	**Genus**																									
Proteobacteria																												
	Alpha-proteobacteria						x		x		x																	
		Beijerinckiaceae																			x			X				
			Methylocapsa										x									x							
			Methylocella										X																
			Methyloferula																										
		Methylocystaceae																											
			Methylocystis					X					x										x			x		x
			Methylosinus										x	x						x		X	X					
			Methylosinus trichosporium																	x		x						
		Upper soil cluster alpha							X	x	x	X															X	x
	Gamma-proteobacteria						X																					
		Methylococcaceae				X													X		X			x				
			Clonothrix																			x						
			Crenothrix																									
			Methylobacter		x				x	x																		
			Methylobacter luteus	X																			x		x			
			Methylobacter psychrophilus											x	x													
			Methylobacter tundripaludum	X	X								x	X	X	X		X										
			Methylocaldum														X						x					
			Methylococcus										x															
			Methylogaea																									
			Methylohalobius						x	x	x																	
			Methylomarinum																									
			Methylomicrobium																									
			Methylomonas																	x					x			
			Methylosarcina																	x					x			
			Methylosoma												x					x								
			Methylosphaera																									
			Methylothermus																	x					x			
			Methylovulum																									
		Upper soil cluster gamma								X																		
Uncharacterized pmoA/amoA										x	X																	
Verrucomicrobia																												
	Verrucomicrobiae																											
		Methylacidiphilaceae																										
			Methylacidiphilum										x															

Notes:
Beige highlighted cells are soil samples with empirical support of atmospheric CH_4 oxidation
Blue highlighted species are known pschrophilic or psychrotolerant methanotrophs
"X" and "x" indicated the presence of methanotrophs in the sample and "X" denotes the most dominant group
Columns to the right of the dotted lines are studies of sub-Arctic regions which are provided as reference
NA: Not available

Table S6. CH_4 oxidation rates (mean±S.E.M.) estimated from microcosm experiments

Incubation condition		**Final [CH4]**	**Rate constant, *k***	**Estimated CH_4 oxidation rate at 1.81 ppmv**	**Estimated CH_4 flux**
Temp. (°C)	**Water saturation (%)**	**(ppmv)**	**(1 (g of soil)$^{-1}$ day^{-1})**	**(ng C (g of soil)$^{-1}$ day^{-1})**	**(mg C m^{-2} day^{-1})**
4	33	0.6	-0.011±0.005 (R^2=0.902)	-2.56±1.22	-0.23±0.11
4	66	1.4	-0.003±0.002 (R^2=0.691)	-0.73±0.49	-0.07±0.04
4	100	1	-0.003±0.001 (R^2=0.796)	-0.70±0.30	-0.06±0.03
10	33	0.1	-0.026±0.006 (R^2=0.861)	-5.90±1.34	-0.53±0.12
10	66	0.6	-0.006±0.001 (R^2=0.821)	-1.26±0.32	-0.11±0.03
10	100	0.4	-0.008±0.004 (R^2=0.762)	-1.81±0.95	-0.16±0.09

Table S7. Methanogenic taxa identified in near-surface cryosols (at 5 cm depth) in the intact core incubation experiment.

Phylum	Class	Family	Genus[1]	Mean % abundance > 0.001% (± std)[2]	Methanogenesis pathway
Euryarchaeota	Methanobacteria	Methanobacteriaceae	*Methanobrevibacter*	0.0011 (±0.0033)	Hydrogenotrophic
Euryarchaeota	Methanobacteria	Methanobacteriaceae	*Methanothermobacter*	0.0107 (±0.0080)	Hydrogenotrophic
Euryarchaeota	Methanobacteria	Methanothermaceae	*Methanothermus*	0.0011 (±0. 0018)	Hydrogenotrophic
Euryarchaeota	Methanococci	Methanocaldococcaceae	*Methanocaldococcus*	0.0052 (±0.0103)	Hydrogenotrophic
Euryarchaeota	Methanococci	Methanococcaceae	*Methanococcus*	0.0034 (±0.0054)	Hydrogenotrophic
Euryarchaeota	Methanococci	Methanocellaceae	*Methanocella*	0.0081 (±0.0065)	Hydrogenotrophic
Euryarchaeota	Methanococci	Methanocorpusculaceae	*Methanocorpusculum*	0.0010 (±0.0270)	Hydrogenotrophic
Euryarchaeota	Methanococci	Methanomicrobiaceae	*Methanoculleus*	0.0035 (±0.0100)	Hydrogenotrophic
Euryarchaeota	Methanococci	Methanospirillaceae	*Methanospirillum*	0.0085 (±0.0123)	Hydrogenotrophic
Euryarchaeota	Methanococci	Methanomicrobiales	*Methanoregula*	0.0163 (±0.0101)	Hydrogenotrophic
Euryarchaeota	Methanococci	Methanomicrobiales	*Methanosphaerula*	0.0120 (±0.0100)	Hydrogenotrophic
Euryarchaeota	Methanococci	Methanosaetaceae	*Methanosaeta*	0.0072 (±0.0071)	Aceticlastic
Euryarchaeota	Methanococci	Methanosarcinaceae	*Methanococcoides*	0.0088 (±0.0056)	Methylotrophic
Euryarchaeota	Methanococci	Methanosarcinaceae	*Methanohalobium*	0.0029(±0.0049)	Methylotrophic
Euryarchaeota	Methanococci	Methanosarcinaceae	*Methanohalophilus*	0.0027 (±0.0023)	Methylotrophic
Euryarchaeota	Methanococci	Methanosarcinaceae	*Methanosarcina*[3]	0.0686 (±0.0263)	Aceticlastic
				Total =0.69%	

Notes:

[1]Genera that were sporadically present in some samples with a relative abundances < 0.001% include: *Methanobacterium, Methanosphaera, Methanothermus, Methanothermococcus, Methanoplanus* and *Methanopyrus*.

[2]Mean abundance of 16 cryosol samples collected at different time during the course of incubation (T=0, 1 week, 6 months and 12 months).

[3]This genus contains representatives that are capable of oxidizing CH_4 anaerobically.